

**UNIVERSITY OF WEST BOHEMIA IN PILSEN  
FACULTY OF ELECTRICAL ENGINEERING**

**Department of technology and measurement**

# **DIPLOMA THESIS**

**Parallel Magnetically Guided Actuation of Ferromagnetic Bodies**

**ZÁPADOČESKÁ UNIVERZITA V PLZNI**  
Fakulta elektrotechnická  
Akademický rok: 2017/2018

**ZADÁNÍ DIPLOMOVÉ PRÁCE**  
(PROJEKTU, UMĚLECKÉHO DÍLA, UMĚLECKÉHO VÝKONU)

Jméno a příjmení: **Bc. Jiří VLČEK**  
Osobní číslo: **E16N0034P**  
Studijní program: **N2612 Elektrotechnika a informatika**  
Studijní obor: **Komerční elektrotechnika**  
Název tématu: **Paralelní polohování feromagnetických těles pomocí magnetického pole**  
Zadávající katedra: **Katedra technologií a měření**

**Z á s a d y p r o v y p r a c o v á n í :**

1. Popište problematiku paralelního prostorového polohování feromagnetických těles pomocí magnetického pole.
2. Proveďte rešerši současných systémů založených na této technice. Zaměřte se především na možnosti jejího využití pro ovládání miniaturních robotických systémů.
3. Formulujte matematický model popisující danou techniku polohování a na základě jeho řešení proveďte počítačovou simulaci.
4. Vytvořte základní návrh systému využívající paralelní polohování miniaturních feromagnetických těles.
5. Ověřte funkčnost navrženého systému na jeho prototypu a navrhnete algoritmy pro jeho řízení.

Rozsah grafických prací: podle doporučení vedoucího

Rozsah kvalifikační práce: 40 - 60 stran

Forma zpracování diplomové práce: tištěná/elektronická

Seznam odborné literatury:

1. LI, Jinxing, et al. Micro/nanorobots for biomedicine: Delivery, surgery, sensing, and detoxification. *Science Robotics*, 2017.
2. ARORA, Nipun, et al. A planar electromagnetic actuator based on two layer coil assembly for micro applications. 2014 IEEE/ASME International Conference on Advanced Intelligent Mechatronics, 2014.
3. RAHMER, Jürgen, et al. Spatially selective remote magnetic actuation of identical helical micromachines. *Science Robotics*, 2017.
4. DANG, The Anh Tuan, et al. Electromagnetic modular Smart Surface architecture and control in a microfactory context. *Computers in Industry*, 2016.
5. BECKER, Aaron, et al. Massive uniform manipulation: Controlling large populations of simple robots with a common input signal. IEEE/RSJ International Conference on Intelligent Robots and Systems (IROS), 2013.

Vedoucí diplomové práce: Ing. František Mach, Ph.D.

Regionální inovační centrum elektrotechniky

Konzultant diplomové práce: Bc. Jiří Kuthan

Datum zadání diplomové práce: 10. října 2017

Termín odevzdání diplomové práce: 24. května 2018

  
Doc. Ing. Jiří Hammerbauer, Ph.D.  
děkan



  
Doc. Ing. Aleš Hamáček, Ph.D.  
vedoucí katedry

V Plzni dne 10. října 2017

## Abstract

This diploma thesis is focused on the introduction of the principle of independent parallel positioning of ferromagnetic bodies by magnetic field. The work builds on the electromagnetic system *MagStriver*, which allowed independent movement of only one robot. The robot is composed of a permanent magnets and is controlled by a set of four coplanar space-shifted coils in two degrees of freedom.

Thesis is divided into seven parts. The first part deals with the definition of basic concepts and motivation. The second summarizes state of the art. The third sets out the main objectives of the work. The fourth part defines mathematical models of the system and deals with the development of a new *Scarabeus* platform that allows independent positioning of only one robot. For which parametric analysis was developed in the simulation software *Agros2D*. The purpose of the analysis was to soften the platform step size, minimize the robot, and maximize the force courses on the robot. The fifth part contains description and experimental verification of the *Scarabeus* system and comparison of properties with its older prototype.

This knowledge was implemented in the sixth and seventh part of the thesis dealing with development of the *Isoptera* platform. These parts successfully solve the main goal of the diploma thesis, namely to design, realization and description of the functional *segmental* system for independent parallel actuation by magnetic field. Independent parallel movement is achieved by differentiate of working area into the self-controlled *segments*.

## Key words

Independent electromagnetic parallel positioning, ferromagnetic bodies, magnetic fields, coils, electromagnetic actuator, miniature robot

## Abstrakt

Předkládaná diplomová práce je zaměřena na seznámení s principy nezávislého paralelního polohování feromagnetických těles magnetickým polem. Práce navazuje na elektromagnetický systém *MagStriver*, jež umožňoval nezávislý pohyb pouze jednoho robota. Robot je složený z permanentních magnetů a je ovládán souborem čtyř koplanárních prostorově posunutých cívek ve dvou stupních volnosti.

Vlastní práce je rozdělena do sedmi částí. První část se zabývá definicí základních pojmů a motivací. Druhá shrnuje současný stav poznání. Třetí stanovuje hlavní cíle práce. Čtvrtá část stanovuje matematické modely systému a zabývá se vývojem nové platformy *Scarabeus* umožňující nezávislé polohování pouze jednoho robota. Pro kterou byly vytvořeny parametrické analýzy v simulačním softwaru *Agros2D*. Účelem analýz bylo zjemnění kroku platformy, minimalizace robota a maximalizace silových průběhů platformy na robota. V páté části je obsažen popis a experimentálním ověřením systému *Scarabeus* a porovnání vlastností s jeho starším prototypem.

Tyto znalosti byly využity v šesté a sedmé části práce zabývající se vývoje platformy *Isoptera*. Ty již úspěšně řeší hlavní cíl diplomové práce, a to návrh, realizaci a popis *segmentového* systému pro nezávislé paralelní polohování elektromagnetickým polem. Nezávislého paralelního pohybu je docíleno rozdělením pracovní plochy na samostatně ovládané *segmenty*.

## Klíčová slova

Nezávislé elektromagnetické paralelní polohování, feromagnetická tělesa, magnetické pole, cívky, elektromagnetický akční člen, miniaturní robot

## **Declaration**

I declare that I have developed this diploma thesis independently, using the professional literature and sources stated in the list, which is part of this diploma thesis.

I further declare that all the software used to resolve this diploma thesis is legal

.....  
signature

## **Acknowledgment**

I would like to express my gratitude to the supervisor of the master thesis Ing. Frantisek Mach Ph.D., for valuable professional advices, comments and methodical work management. To my colleagues Ing. Jiří Kuthan and Ing. Martin Juřík, for professional advices, comments and to work contribution. To the entire team of developers who created the *Agros2D* software and finally my biggest gratitude belongs to my beloved family which supported my through all difficulties which occurred during my lifetime. Thesis especially is dedicated to my grandfather.

# Content

<b>CONTENT</b> .....	<b>8</b>
<b>LIST OF SYMBOLS AND SHORTCUTS</b> .....	<b>9</b>
<b>1 INTRODUCTION</b> .....	<b>11</b>
1.1 DEFINITION OF BASIC CONCEPTS .....	11
1.2 MOTIVATION .....	13
<b>2 STATE OF THE ART</b> .....	<b>14</b>
2.1 PLANAR SINGLE ROBOT SYSTEMS .....	15
2.1.1 <i>MagStrive</i> platform .....	15
2.1.2 <i>MagPier</i> platform .....	17
2.2 PLANAR SYSTEMS WITH INDEPENDENT PARALLEL MAGNETIC ACTUATION .....	18
2.2.1 <i>MicroFactory</i> platform for Smart Manufacturing .....	18
2.2.2 <i>MagMan</i> platform .....	20
<b>3 THE MAIN THESIS OBJECTIVES</b> .....	<b>21</b>
<b>4 DESIGN OF <i>SCARABEUS</i> PLATFORM</b> .....	<b>22</b>
4.1 MATHEMATICAL MODEL OF MAGNETIC FIELD .....	22
4.1.1 Research of Maxwell and Lorentz forces .....	24
4.1.2 Study of magnetic force dependency on magnet width .....	26
4.1.3 Study of magnetic force dependency on the gap - wire width ratio .....	29
4.2 MATHEMATICAL MODEL OF MOTION .....	33
4.3 ROBOT BODY DESIGN .....	34
<b>5 <i>SCARABEUS</i> PLATFORM SPECIFICATION</b> .....	<b>35</b>
5.1 PRINCIPLE OF ROBOT CONTROL .....	36
5.2 HARDWARE AND CONTROL ALGORITHM .....	39
5.3 EXPERIMENTAL VERIFICATION .....	40
5.3.1 Robot motion analysis .....	40
5.3.2 Interaction between two robots .....	41
5.3.3 Interaction between robot and ferromagnetic body .....	42
5.3.4 Identification of dynamic characteristics .....	43
5.3.5 Analysis of transport capabilities .....	44
5.4 COMPARISON BETWEEN <i>MAGSTRIVER</i> AND <i>SCARABEUS PLATFORM</i> .....	45
<b>6 DESIGN OF <i>ISOPTERA</i> PLATFORM</b> .....	<b>46</b>
6.1 COILS RESISTANCE REDUCTION .....	46
<b>7 <i>ISOPTERA</i> PLATFORM SPECIFICATION</b> .....	<b>48</b>
7.1 BLOCK DIAGRAM, HARDWARE AND CONTROL ALGORITHM .....	50
7.2 EXPERIMENTAL VERIFICATION OF CROSSOVERS .....	52
<b>8 CONCLUSION</b> .....	<b>56</b>
<b>LIST OF LITERATURE AND INFORMATION SOURCES</b> .....	<b>58</b>
<b>ANNEX</b> .....	<b>1</b>
CONTROL ALGORITHM FLOWCHART OF THE <i>ISOPTERA</i> PLATFORM .....	1

## List of symbols and shortcuts

MAS	Multi-agent system	
ABS	Acrylonitrile butadiene styrene	
UWB	University of West Bohemia	
CTU	Czech Technical University in Prague	
PCB	Printed Circuit Board	
DM3	Diamagnetic Micro Manipulation	
PM	Permanent magnet	
PLA	Polylactid acid	
DOF	Degrees of freedom	
CNC	Computer Numeric Control	
LED	Light Emitting Diode	
$\mu$	permeability	H.m <sup>-1</sup>
$\mu_r$	relative permeability	-
$\gamma$	electric conduction	S.m <sup>-1</sup>
$\rho$	electric resistivity	$\Omega$ .m <sup>-1</sup>
$\Omega$	definition area	-
$\Gamma$	boundary condition	-
$\otimes$	dyadic product	
$\sigma_M$	Maxwell stress tensor	
$a$	acceleration	m.s <sup>-2</sup>
$A$	magnetic potential	Wb.m <sup>-1</sup>
$B$	flux density	T
$B_r$	remanent flux density	T
$E$	electric field strength	V.m <sup>-1</sup>
$F$	force	N
$F_L$	Lorentz force	N
$F_M$	Maxwell force	N
$F_{Mx}$	electromagnetic force in the x direction	N
$F_{Mz}$	electromagnetic force in the z direction	N
$F_t$	friction force	N
$g$	insulation gap width	mm

$g$	gravitational constant	$\text{m}\cdot\text{s}^{-2}$
$J_{\text{ext}}$	external current density	$\text{A}\cdot\text{m}^{-2}$
$I$	electric current	A
$\mathbf{I}$	unit matrix	
$k$	coefficient of shear friction	-
$L_{1-4}$	coils 1-4	
$m_{1-6}$	magnet widths	mm
$m$	mass	kg
$Q$	electric charge	C
$R$	resistance	$\Omega$
$S$	cross section area	$\text{mm}^2$
$S_S$	cross section area of <i>Scarabeus</i> 's coils	$\text{mm}^2$
$S_M$	cross section area of <i>MagStriver</i> 's coils	$\text{mm}^2$
$t$	time	s
$v$	velocity	$\text{m}\cdot\text{s}^{-1}$
$w$	wire width	mm
$wh$	wire height	mm
$ww$	wire width	mm

# 1 Introduction

## 1.1 Definition of basic concepts

Term micro-factory was first introduced and proposed by the Mechanical Engineer Laboratory of Japan in 1990. Concept micro refers to small dimension factory able to produce small dimension products. Due to their reduced size micro-factories should be highly automated and be equipped with machine tools, assembly, quality inspection , material feed, waste elimination and tool replacing systems. [1]

For many years, micro and mini multi-agent systems of multiple or many robots have been investigated. For instance, as in nature. Species like ants and bees are able to build impressive structures thanks to their collective cooperation. The same holds for multi-agent systems. Multi-agent system (MAS) is a simulated environment of a network character whose elements interact through certain types of agents with each other and / or the environment in which they are located. These agents solve together problems that go beyond the possibilities and knowledge of each one. These robot systems can achieve significant benefits in comparison with their single working relatives. [2][3]

A number of techniques are currently being developed to allow the manipulation of bodies on spatial scales ranging from millimeters to nanometers. Potential applications of systems using these techniques are extensive and in range from minimal invasive treatment procedures through manipulation of laboratory samples to technology of production and processing of microscopic and macroscopic products. [4]

The term *microactuator* has its history of microengineering. It is microengineering itself that has evolved to create the most widely used sensors (pressure and acceleration) in micrometre units. Microsensors are used in a large variety of parts, such as gyroscopes and electric transducers quantities other than electric. *Microactuator* is a term for an element that performs exactly the opposite function of the microsensor. It converts the input energy, which is mostly electric, to mechanical energy. At present, microarrays are produced such as micro pumps, microswitches, micromotors or micromanipulator. [5]

Techniques of micromanipulation are based on numerous physical principles. Examples which ensure movement actuation itself, include for example, acoustic field control, optical bundle, chemical reaction or biochemical process or electric and magnetic field. Electric field control is mainly used for spatial scales in the order of micrometres, nowadays almost exclusively in the field of manipulation of laboratory samples. The magnetic field can then be used primarily in applications where manipulation of bodies with a size from micrometres to millimetres is required, with a very high accuracy. [4]

The basic principle of magnetic control is the force effect of the controlled magnetic field on actuated ferromagnetic bodies, most often permanent magnets. Also ferromagnetic bodies usually fitted in a plastic profiles are in these platforms defined as robots. Developed systems differ primarily according to the coil topology used to create a magnetic field. Robot movement is then always achieved by temporal and spatial change in the magnetic field distribution. This can be achieved by varying the magnitude of the excitation current in individual coils or by their cyclic switching. These systems include *MagMan* [6], developed at the CTU in Prague, or *MagStriver* [7] at the UWB in Pilsen. [4]

## 1.2 Motivation

The work starts from the diploma thesis written by Ing. Jiří Kuthan under leadership of Ing. František Mach Ph.D, who one year ago started a project dealing with electromagnetic actuation platforms called *MagSnail* and *MagStriver* [7]. The *MagSnail* platform is the first generation of prototype, which served for principle verification and next knowledge is built on the generation of system *MagStriver*. Obtained knowledge could be implemented later in dissertation work of Ing. Jiří Kuthan, which also deals with similar topic of parallel magnetic actuation. The mentioned technology provides positioning of robot by actuators with two degrees of freedom ( $x$ - $y$  directions). Robots are made from plastic profile equipped with neodymium magnets. The system proved to be functional and shown its excessive potential in meso-manipulation scales, especially in accuracy of controlling mini robot and its capacity load due to its size and weight.

Unfortunately, the system has not been able to control more than one ferromagnetic body separately at once. For its great properties, however, further extension of research has been suggested. This deals with possibility to use principles of the mentioned *MagStriver* platform to control more than one robot in parallel. In order to deal with problems of parallel actuation, the work contains research of currently used systems, description of parallel movement problematics, parametric analysis, platform layout, control system design and experimental verification.

The main objectives builds on the development of a new platform which allows independent parallel actuating multiple robots. And other sub-goals are minimization and optimization of the platform for improvement of the production possibilities. The objectives are described in the Chap. 3 in more detail.

## 2 State of the art

Systems for electromagnetic actuation can be differentiated according to degrees of freedom (DOF) to planar and spatial systems. But also by ability to control a higher number of robots in parallel independently. For continuation of the *MagStriver* system development, we will focus mainly on the possibilities of the planar actuation. Well-known techniques will be summarized in the followed paragraphs.

Most of current systems for magnetically guided actuations are based on the electromagnetic force principles. The forces act among ferromagnetic bodies, especially among permanent magnets (PM). These systems differentiate by the coils topology, materials and shapes of actuated bodies and, of course, in their operation and motion. A few current systems and their basic principles are illustrated in Fig. 1. Also, it has to be noted that the chosen principles do not cover all known technical solutions, but usually many of them use similar principle or their variations. An arena also means working area of the platform.[8]

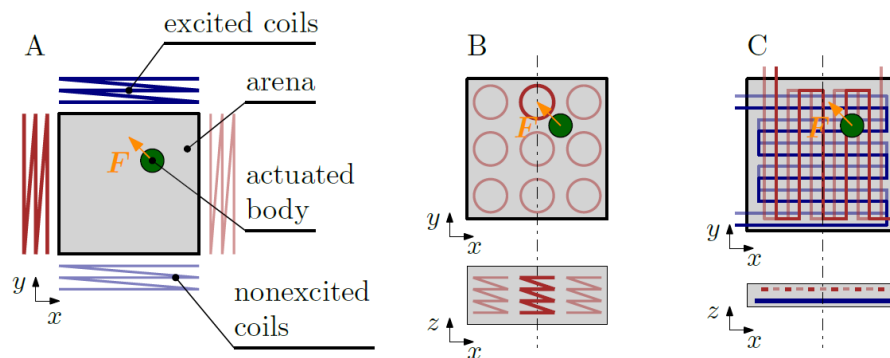


Fig. 1. Illustration of the basic system variations, which are dealing with magnetically guided actuation of ferromagnetic bodies on the planar surfaces. Guided actuation is achieved by different positioning of actuated coils. System uses concentrated coils: A) outside of arena, B) perpendicular coils under the arena, C) coplanar coils under the arena. [8]

## 2.1 Planar single robot systems

First of all, two basic systems will be introduced which deal with independent magnetically guided actuation of only one robot.

### 2.1.1 *MagStriver* platform

The system and its principle was researched and further developed in the University of West Bohemia. Unfortunately, the system does not support independent parallel magnetically guided actuation. The layout can be seen in Fig. 2. Periodical current switching of red (top layer) coils causes nonzero circulation of magnetic field and occurs in interaction with stationary magnetic field of permanent magnets embedded in the plastic profile (robot). The interaction creates force which enables robot movement along the  $x$ -axis. (Fig. 3) The same principle is used for blue (bottom layer) coils and magnets except in direction of  $y$ -axis, caused by coils rotated by  $90^\circ$ . Also robots' magnets poles have to be placed in specific direction, but there should be used a different way and combinations of magnets, and also their shape. [7]

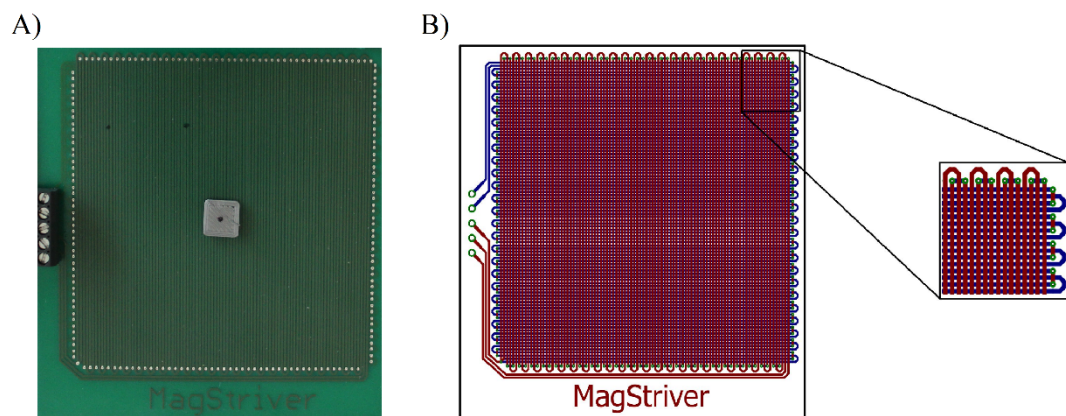


Fig. 2. Illustration of *MagStriver* platform. A) Photograph of working area with robot; B) Layout design with detailed cut out of conductive traces interconnection. [7]

Also *MagStriver* platform is based on its larger prototype and the first generation system called *MagSnail*. During its design, the main motivations for its research was dimension reduction, step softening, reducing the error rate and doing it all in order to achieve the smallest possible currents and voltages. The platform focused on the production simplicity with minimal costs. The design was made up of a 0.5 mm wide conductor with an insulation gap 0.25 mm.[7]

Graphical principle is shown in Fig. 3, which illustrates a robot actuation cycle and movement. Further explanation of working principle will be discussed in Chapt. 5.1, that also describes the technique of actuation with *lock-up field*. [7]

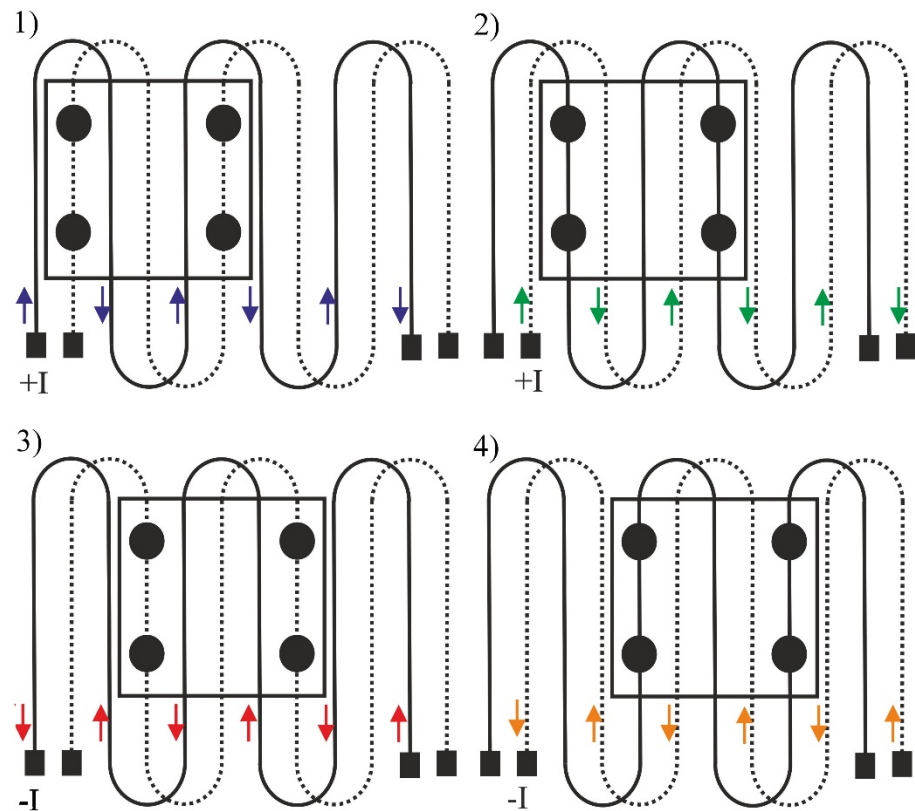


Fig. 3. Description of the current flow and robot's movement in each step. 1) Phase one: the first coil enabled. 2) Phase two: the second coil enabled. 3) Phase three: the first coil inversely enabled 4) Phase four: the second coil inversely enabled. [7]

The robots for *MagStriver* platform were printed from ABS plastic on 3D printer and subsequently fitted with cylindrical 1x1 mm neodymium magnets. There are three types of robots shown in Fig. 4 that were created to fit four or nine magnets. The dimensions of four-magnet robot are 5.5 x 5.5 mm and 8.6 x 8.6 mm. (Fig. 4 B and C) The larger dimension (8.6 x 8.6 mm) robot also fits for nine magnets. (Fig. 4 A) [7]

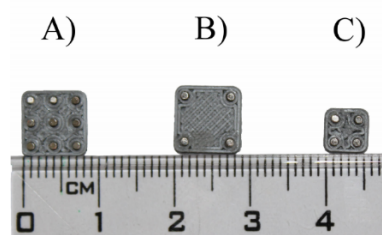


Fig. 4. Different types of robots for *MagStriver* platform. A) The robot with nine PMs, B) The robot with four PMs with greater pitch. C) The small robot with four PMs. [7]

Also for the correct system function, the pitch between magnets has to match conductor traces, which carry current of the same direction as shown in Fig. 5.

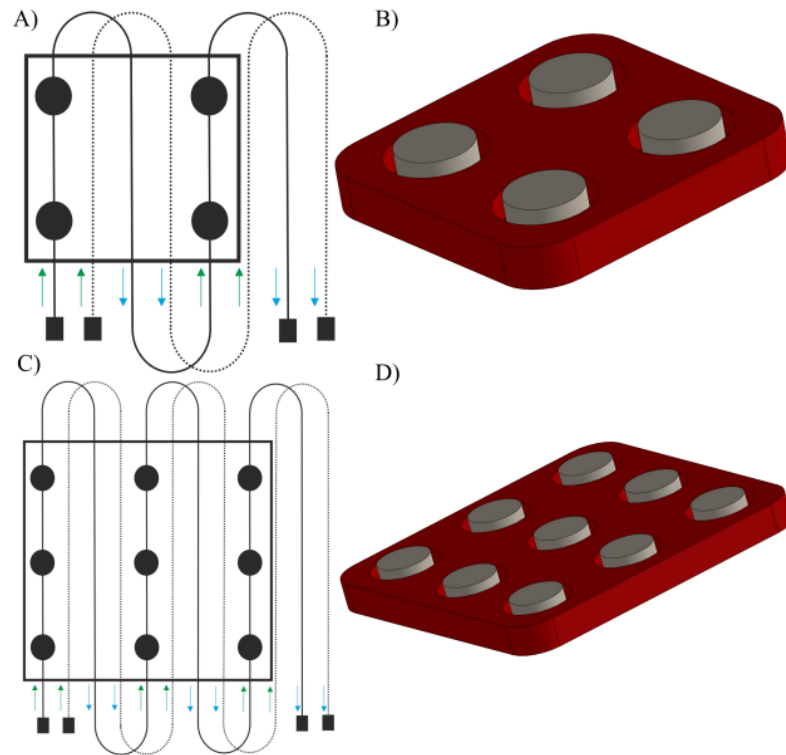


Fig. 5. A) Distance between magnets of four-magnet robot; B) Sample of four-magnet robot; C) Distance between magnets of nine-magnet robot; D) Sample of nine-magnet robot. [7]

### 2.1.2 *MagPier* platform

Another planar system is called *MagPier*. It belongs between the fastest planar systems. *MagPier* won 2 mm sprint in 2011 introduced by the IEEE International Conference on robotics and Automation (ICEM 2011). System uses combination of electromagnetic field and piezoelectric effect. Ferromagnetic body is moved by four coils, which are spatially rotated by 90. (Fig. 6). These coils generate electromagnetic field which enables accurate planar movement. Also mini robot can move without adhesive force only with reduced friction. This effect is based on the piezoelectric principle. The effect is caused by the high-voltage electrode, which is connected to a source of voltage of 300 V with frequency of 100 Hz. The robot is made of ferromagnetic and piezoelectric materials. (Fig. 6 C) [9]

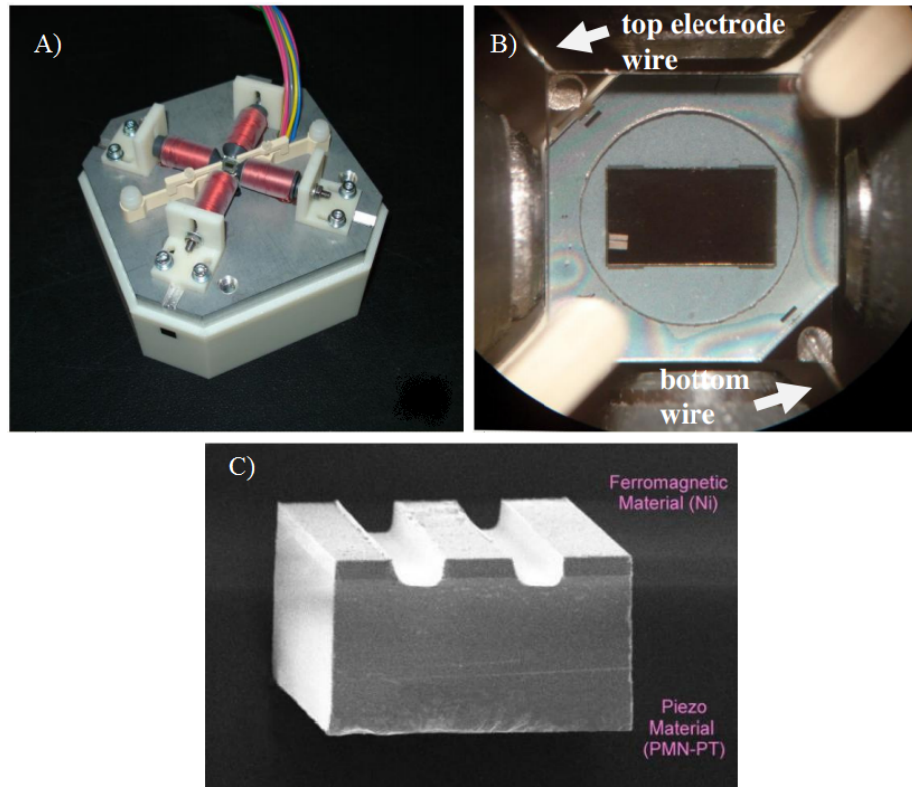


Fig. 6. Illustration of the *MagPier* platform A) Photograph of *MagPier* four coil platform. Total system size is  $11 \times 11 \text{ cm}^2$ . B) Photograph of the working arena. C) Photograph of the robot type I.2 used for system *MagPier* made from piezo and ferromagnetic material. [9]

## 2.2 Planar systems with independent parallel magnetic actuation

The magnetic actuation MAS are one of the most challenging topics of nowadays. This chapter summarizes and describes two platforms which are able to use independent parallel magnetically guided actuation of multiple ferromagnetic bodies.

### 2.2.1 *MicroFactory* platform for Smart Manufacturing

SRI's micro-robots are controlled by magnetic field generated by the printed circuit board substrate. With use of technology Diamagnetic Micro Manipulation (DM3) in a multi-agent context. The concept micro in this case refers to small dimensions. (Fig. 7) [10]

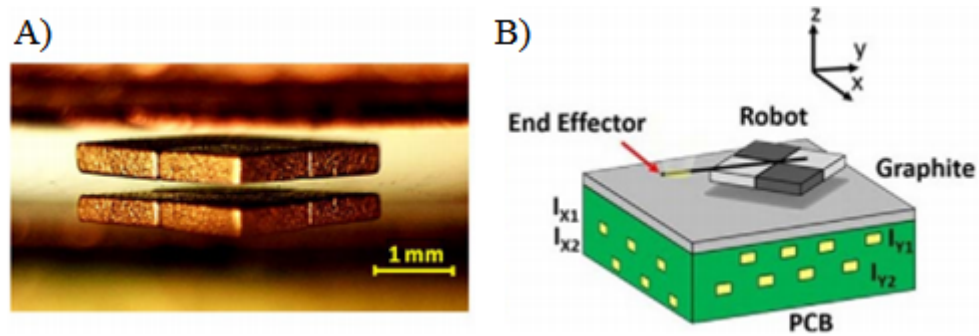


Fig. 7. Illustration of SRI's *Microfactory* platform. A) Levitated robot photograph of a DM3 system. B) Illustrated principle of DM3 system [10]

Current switching through specific traces drives the robot with two degrees of freedom ( $x$ - $y$  trajectory). The diamagnetic graphite layer creates the passive levitation force due to repelling force between diamagnetic layer and robot's ferromagnetic body (checkerboard pattern). [10]

Parallel actuation of DM3 system is achieved by multiple working areas (so called segments) controlled separately. Segments use the same principle for generating magnetic flux density, which causes robot's motion. Four coils allow moving in  $x$  and  $y$  directions. Each segment allows one robot moving separately. If more than one robot occurs in one segment, robots moves simultaneously in the same direction until one of them reaches another independently controlled segment. Due to MAS it could be created manufacturing system with hundreds of working robots, which exceeds single robot system possibilities. [10]

The only difference between those two systems consists in the mentioned coating of PCB surface with diamagnetic material. SRI uses diamagnetic properties of graphite layer. Coating repels robot's ferromagnetic body in order to eliminate or reduce friction force. Graphite thickness causes difference between elimination and reduction of friction. 0.5 mm wide layer causes levitation, while 25 to 100  $\mu\text{m}$  wide layer is used for diamagnetic sliding systems. [10]

The SRI's mini- or micro-robots can be very fast. Maximum speed reached so far is 55 cm/s. Also robots can climb straight up walls or travel on flex circuits in any orientation. By adding end effectors (simple as metal wires) the micro-robots can perform useful tasks. For instance, they can carry thin carbon rods, which is used for manufacturing high strength and low weight structures like trusses. SRI's successfully created truss structures are long up to 29 cm and able to hold up to 1 kg. [10]

### 2.2.2 *MagMan* platform

This section describes the *MagMan* platform developed by CTU in Prague, which contains all necessary information. For the sake of simplicity, the platform is composed from two units: an array of coils and a surface placed on the top of the array. If the coil is excited, the surrounding magnetic field affects the ferromagnetic body by an attractive force. If coils are excited in specific order, magnetic field can create controlled motion of ferromagnetic body, for example a steel ball. [6]

The platform allows two solutions of the position measurement. The first one uses an RGB camera, which captures steel ball movement. The second one uses a resistive touch foil, which is laid down on the top horizontal layer of the planar surface. [6]

The array of the coils is made from modules, every single module consists four coils with iron cores. The module dimensions are 50 x 50 mm<sup>2</sup> shaped from the top view. Each module is under the working surface with an electronic board equipped with an ARM processor. The control of the current through the each module's coils is achieved by electronic circuitry with feedback loop. Photograph of a single module is shown in Fig. 8a. The array unit can be also viewed as smart actuator, because each module has its own computing power and ability to communicate with adjacent units. The whole platform is currently assembled from the four interconnected modules, which forms a 4 x 4 coil's square array. It is depicted in Fig. 8b. [6]

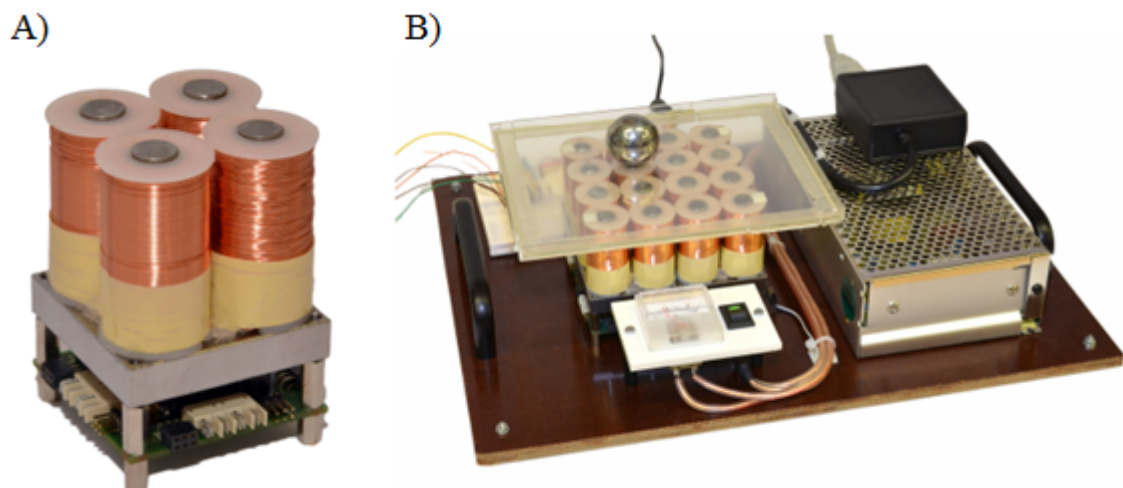


Fig. 8. Photographs illustrating *MagMan* platform a) *MagMan* single module; b) *MagMan* laboratory platform containing four single modules and steel ball. [6]

### 3 The main thesis objectives

The main objectives in the first stage of thesis development were following:

1. Research on independent parallel movement solutions
2. Analysis of researched techniques and possibility of their implementation.

The second stage of third generation development were composed from:

1. Dimension minimization, force maximization through parametric analysis
2. Design of platform prototype for independent movement of one robot based on the parametric analysis.
3. Experimental verification of the prototype function.

The third stage development of the multi-agent system prototype so-called *Isoptera*:

1. Verification and selection of the methods enabling independent parallel movement.
2. Design of the *Isoptera* platform.
3. Experimental function verification, conclusion drawings and planned completion of the project.

## 4 Design of *Scarabeus* platform

For design of new *Scarabeus* platform prototype there was assigned the main goal to reach the smallest dimensions with performance preservation or better its maximization. In order to fulfil these objectives, first a study of Lorentz and Maxwell forces had to be performed, due to missing comprehension of their shares in the system.

### 4.1 Mathematical model of magnetic field

Simulations are performed in software Agros2D [11], containing a mathematical model of magnetic field described by the partial differential equation

$$\operatorname{rot} \left( \frac{1}{\mu} (\operatorname{rot} (\mathbf{A} - \mathbf{B}_r)) \right) - \gamma \mathbf{v} \times \operatorname{rot} \mathbf{A} + \gamma \frac{\partial \mathbf{A}}{\partial t} = \mathbf{J}_{\text{ext}}, \quad (1)$$

where  $\mu$  indicates the permeability,  $\mathbf{A}$  stands for the magnetic vector potential,  $\mathbf{B}_r$  is the remanent flux density,  $\gamma$  is the electric conductivity,  $\mathbf{v}$  is the velocity and  $\mathbf{J}_{\text{ext}}$  is the external current density. Due to small velocity and time variation of magnetic vector potential  $\mathbf{A}$ , the second and third terms in the equation are neglected, which leads to the final form

$$\operatorname{rot} \left( \frac{1}{\mu} (\operatorname{rot} (\mathbf{A} - \mathbf{B}_r)) \right) = \mathbf{J}_{\text{ext}}. \quad (2)$$

Next, it is necessary to determine the model's definition area shown in Fig. 9. The definition area consists of different objects with their specific properties and boundary conditions. In this case,  $\Omega_1$  stands for air,  $\Omega_2$  is the magnet and  $\Omega_3$ – $\Omega_5$  represent differently powered coils. More precisely,  $\Omega_3$  represents the coils without current,  $\Omega_4$  coils with the positive and  $\Omega_5$  for the negative current. Air is closed by a fictitious boundary  $\Gamma_1$ , described by the Dirichlet boundary condition  $\mathbf{A} = \mathbf{0}$ .

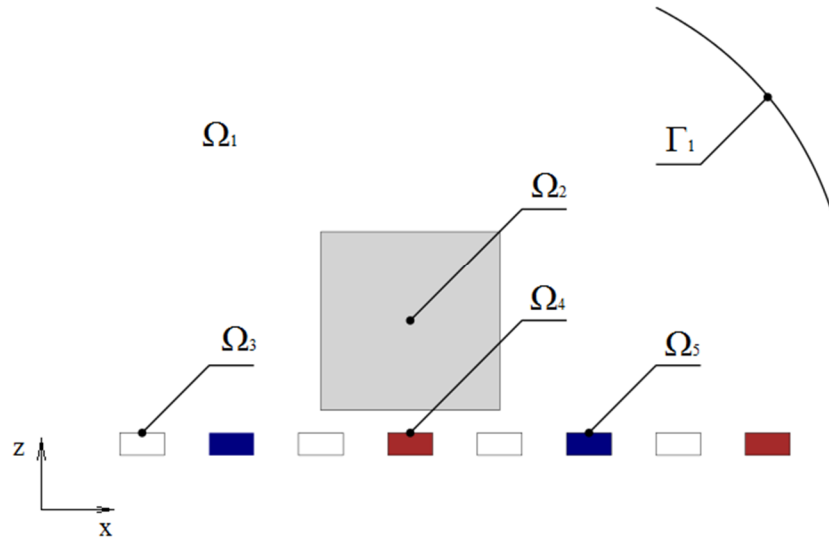


Fig. 9. Definition area of mathematical model describing magnetic field.

Tab. 1. Properties of definition areas.

Definition areas	$\Omega_1$	$\Omega_2$	$\Omega_3$	$\Omega_4$	$\Omega_5$
$\mu_r$ [-]	1	1.05	1	1	1
$B_r$ [T]	0	1.2	0	0	0
$I_{\text{ext}}$ [A]*	0	0	0	+1	-1

The *Agros2D* allows user setting up as material parameter the external current  $I_{\text{ext}}$  and internally calculates the current density  $J_{\text{ext}}$  as

$$J_{\text{ext}} = \frac{I_{\text{ext}}}{S}, \quad (3)$$

where  $S$  is the cross section of the corresponding material.

For studies shown further in this chapter, it is also used tool inside of *Agros2D* called *Serial calculations*. It allows choosing specific labels, edges or nodes and displace, rotate or scale them as needed by given number of iterations. In each iteration are then computed preselected properties of local values, surface and also volume integrals. Also the number of iterations between the starting and target coordinates should be high enough to obtain the finest and most accurate force values.

For studies, displacement of permanent magnet edges and labels are used in order to acquire surface integrals of the Maxwell forces and in the opposite displacement of coil edges and labels to obtain their surface integrals providing the Lorentz forces.

### 4.1.1 Research of Maxwell and Lorentz forces

This chapter summarizes simulations performed in software *Agros2D* supplemented with *Serial calculations* on the designed mathematical model in order to understand the working principle. System uses two types of electromagnetic force called Lorentz and Maxwell force, which both are acquired by different principles.

The values of Lorentz force can be obtained from the expression

$$\mathbf{F}_L = Q(\mathbf{E} + \mathbf{v} \times \mathbf{B}), \quad (4)$$

where  $\mathbf{F}_L$  is the Lorentz force,  $Q$  is the electric charge,  $\mathbf{E}$  is the electric field strength,  $\mathbf{v}$  is the velocity and  $\mathbf{B}$  is the magnetic flux density. Calculation of the Lorentz force in *Agros2D* starts from the formula describing its volumetric value

$$\mathbf{F}_L = \mathbf{J} \times \mathbf{B}, \quad (5)$$

In order to understand Maxwell force, first we need to define the Maxwell stress tensor  $\sigma_M$ , which expresses the flow of momentum of the electromagnetic field over the surface and can be written as

$$\sigma_M = -\frac{1}{2\mu}(\mathbf{B} \cdot \mathbf{B})\mathbf{I} + \frac{1}{\mu}\mathbf{B} \otimes \mathbf{B}, \quad (6)$$

where  $\mathbf{I}$  is a unit matrix and symbol  $\otimes$  represents the dyadic product. [12] Also, in order to successfully calculate Maxwell stress tensor, magnet's remanent flux density must be equal to zero. Otherwise method also includes effect of Lorentz force.

Maxwell force is then defined as

$$\mathbf{F}_M = \int_S \sigma_M d\mathbf{S}, \quad (7)$$

where  $\mathbf{F}_M$  is Maxwell force. [12] Maxwell force acts on the ferromagnetic body and causes its movement in both  $x$  and  $z$  directions. Also, in order to get the Maxwell force values we must simulate the movement of the magnet in the  $x$  coordinate from the initial position of the first powered coil into the position of the second disabled coil. In this case, magnet is moving about one step (from the excited coil A to the stable position of non-excited coil B) relatively to the

stationary position of PCB. (Fig. 10)

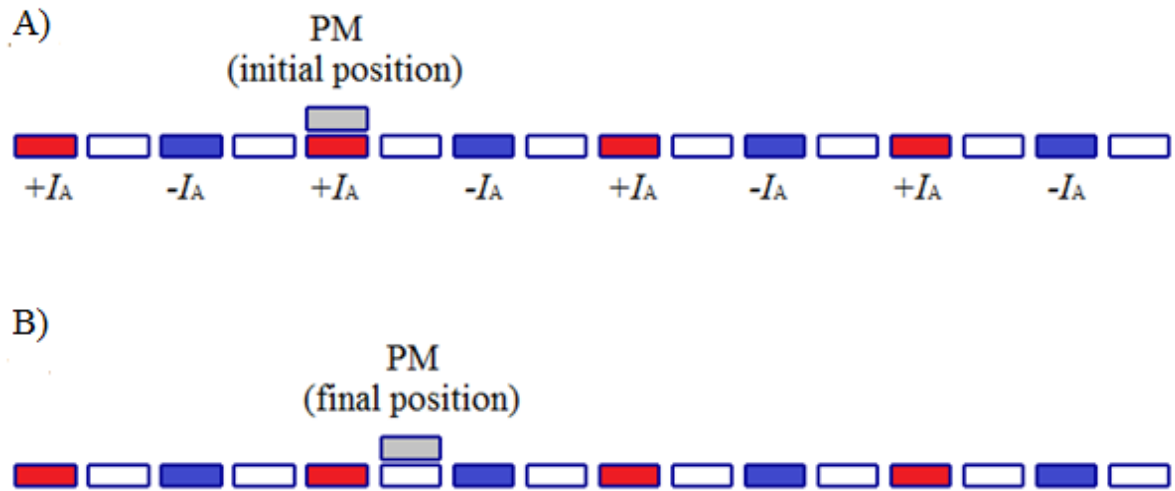


Fig. 10. Example demonstrates one step shift of the PM due to stationary position of PCB.

A) PM in the initial position with excited coil (blue and red rectangles) whose force effect pushes magnet to the position of non-excited coil (white rectangles).

B) PM after one-step shift in the final position after last iteration of *Serial calculations*.

On the contrary, as Maxwell force affects ferromagnetic bodies, the magnet reacts with the Lorentz force on the excited coils. In order to receive these Lorentz force values, the ferromagnetic body has to be in stationary position unlike the powered coils. So force course of one step is obtained by moving coils, while the magnet remains motionless. (Fig. 11)

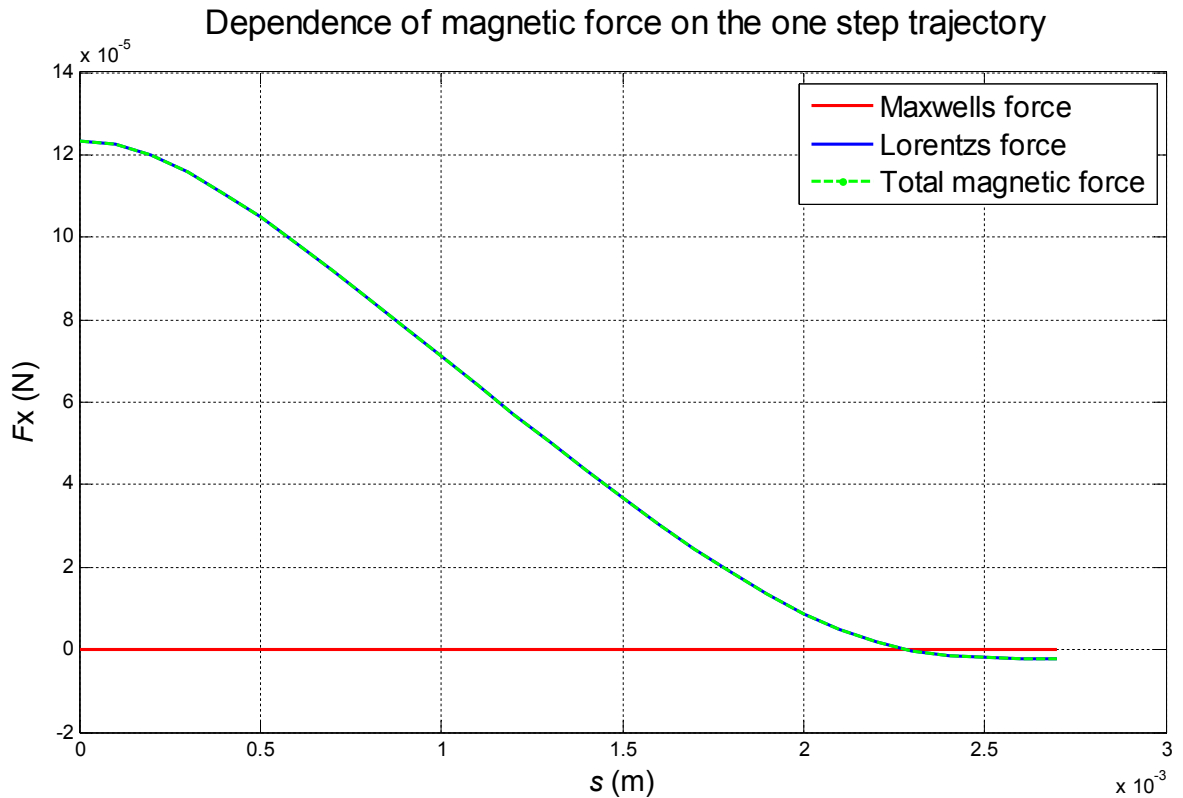


Fig. 11. Shares of the Maxwell and Lorentz  $x$ -axis force courses and their sum.

Figure 11 illustrates the evolution of the Maxwell and Lorentz forces in the system. The highest impact for system motion has the Lorentz force, which pushes magnet away from the excited coils. On the contrary, the Maxwell force is so low, that for further simulations it can be neglected. In following studies, the total magnetic force will be taken into account, which is the sum of both above forces.

#### 4.1.2 Study of magnetic force dependency on magnet width

This chapter summarizes electromagnetic force courses in dependency on the magnet width in  $x$  and  $z$  coordinates with constant wire-gap width ratio. As in the previous simulations, the robot is moved only by one step from the initial position A to the final stable position B. The stated properties are illustrated in Fig. 12.

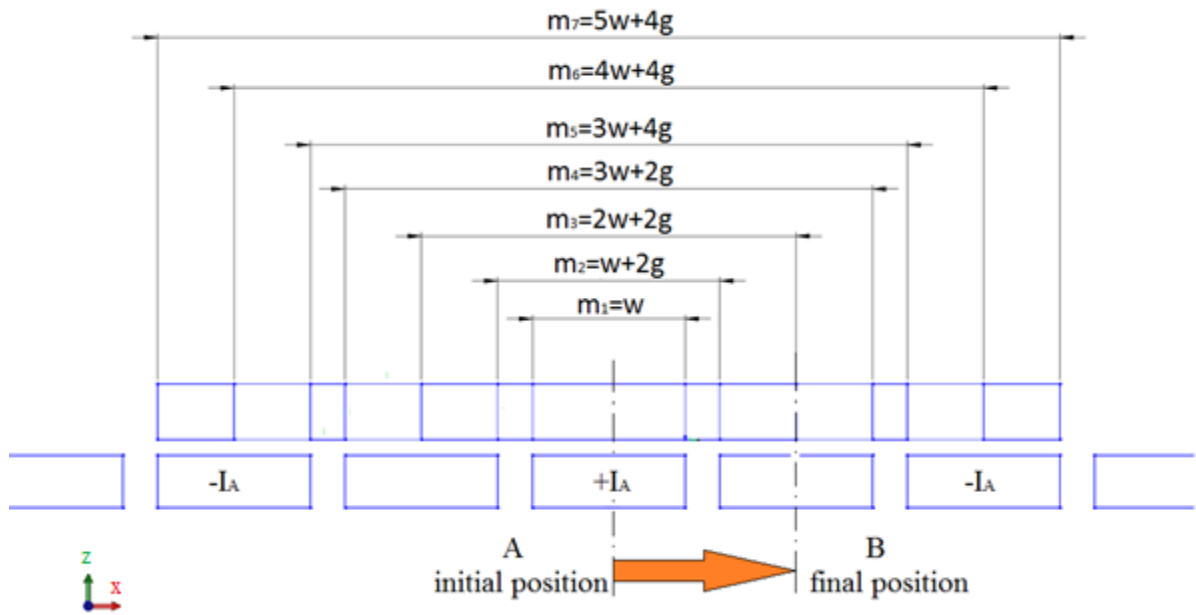


Fig. 12. Magnet widths from  $m_1$  to  $m_7$  for which were performed simulated courses. Each magnet width is described by equation which corresponds to wire and insulation gap widths.

Results of magnetic  $x$ -axis force courses, which were simulated for each magnet width are shown in Fig. 13. The same results for electromagnetic  $z$ -axis force are illustrated in Fig. 14.

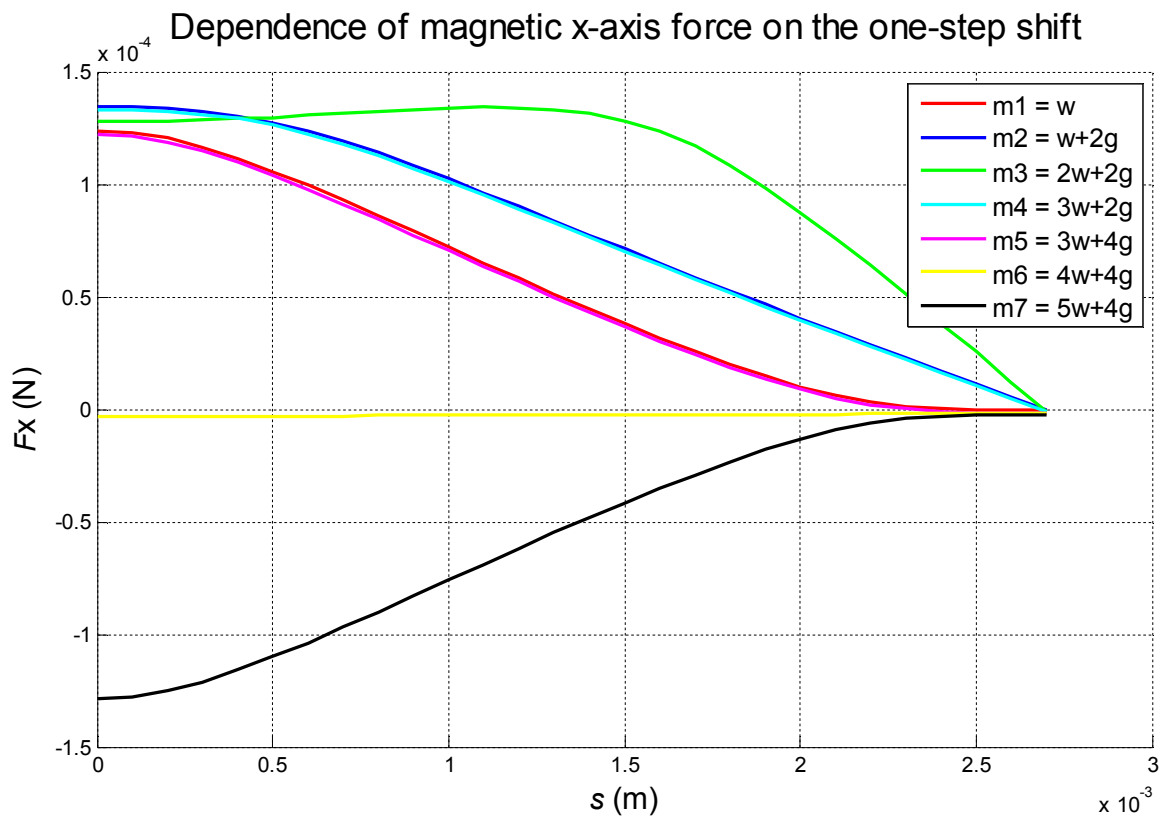


Fig. 13. Magnetic  $x$ -axis force courses for different magnets widths. Shift for each course is done by one step from the excited to the non-excited coil.

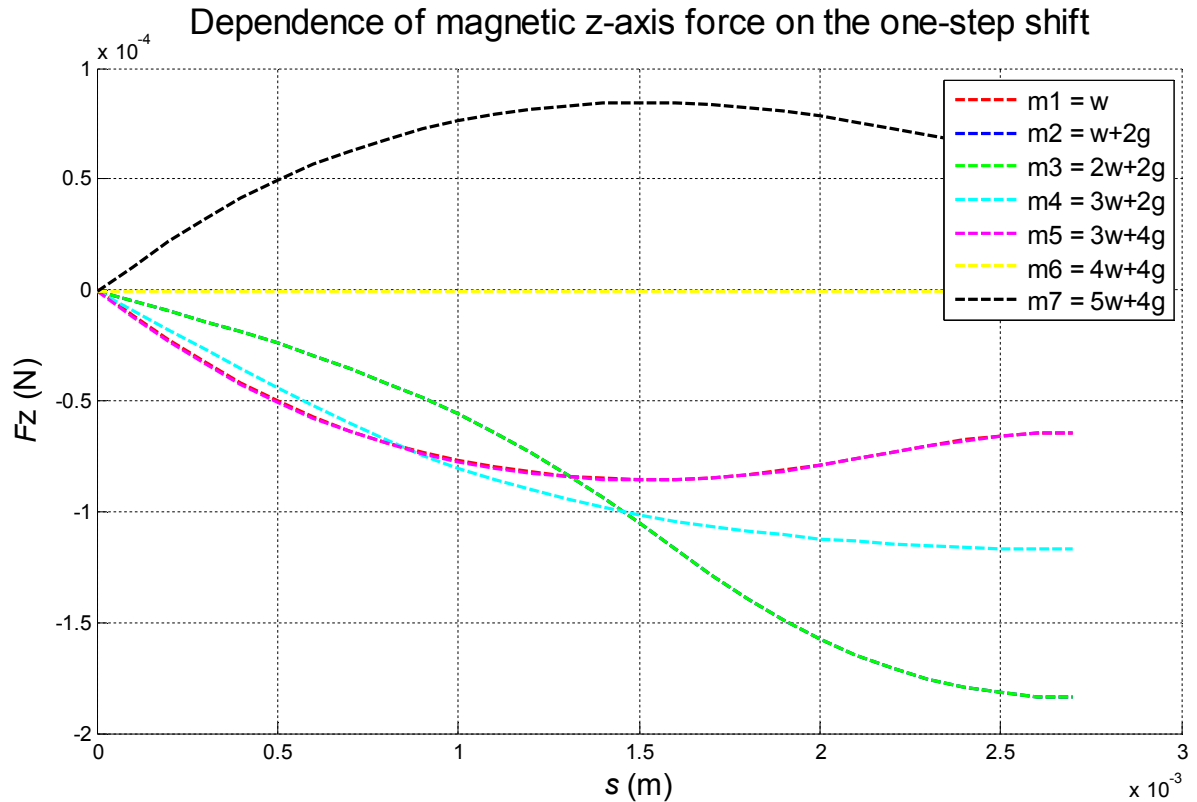


Fig. 14. Magnetic  $z$ -axis force courses for different magnets widths. Shift for each course is done by one step from the excited to the non-excited coil.

As Figs. 13 and 14 show, the system can work almost for every magnet width except  $m_6$  force course. Width  $m_6$  shows a breaking point, which distinguishes robot movement direction in both coordinates. Also the system will not be able to work properly, due to zero force effect which is given by magnet width covering two traces of the same oppositely excited coil.

For our purposes and further research we considered the course of  $m_3$  magnet width with the highest force effect in the  $x$  coordinates, which also has the greatest downforce implied on magnet in stabilized position of the  $z$  coordinate. It is given by the magnet area which has the most effective interaction with one coil trace without additional disturbing force acts created by oppositely excited threads. This  $m_3$  magnet width is equal to two widths of wire and two widths of gap. This rule is crucial for system design.

The system also works with every magnet width (except for the widths around  $m_6$ , which are periodically repeated), till the force overcomes friction force  $F_t$  of the magnet (given mainly by the mass of the magnet).

### 4.1.3 Study of magnetic force dependency on the gap - wire width ratio

This simulation is based on equation acquired by previous study

$$m = 2w + 2g, \quad (8)$$

where  $m$  is magnet width,  $w$  is wire width,  $g$  is insulation gap width.

For established geometric equation (8) it was found the maximal force effect, which acts on the magnet. Simulation also has the same objective and it uses the same principle for computing electromagnetic force courses as previous research. Even the objective remains the same and it again searches for the maximal force effect course, but currently in dependence on the different wire and insulation gap width ratio with constant magnet width.

For stated simulation it was written a computing script attached on the CD, which greatly speeds up the design process. The script enables to quickly set the parameters and directly exports the required variables.

Using the script, it was firstly performed simulations on the general mathematical model, which searched for trends in force course and then control calculations were done for real parameters of *Scarabeus* platform.

Parameters of the general model come from constant magnet width 5.4 mm with five selected wire widths. Widths of remaining insulation gaps are calculated by equation (8). The geometric parameters for general model are listed in Table 2.

Tab. 2: The general model parameters used in simulations.

General model				
width [mm]			height [mm]	
magnet	wire	insulation gap	wire	magnet
5.4	0.5	2.2	0.75	0.75
	1	1.7		
	1.5	1.2		
	2	0.7		
	2.5	0.2		

The simulation results in  $x$  and  $z$  coordinates are shown in the Figs. 15 and 16.

Dependence of magnetic  $x$ -axis force on the one-step shift with changing wire-gap ratio

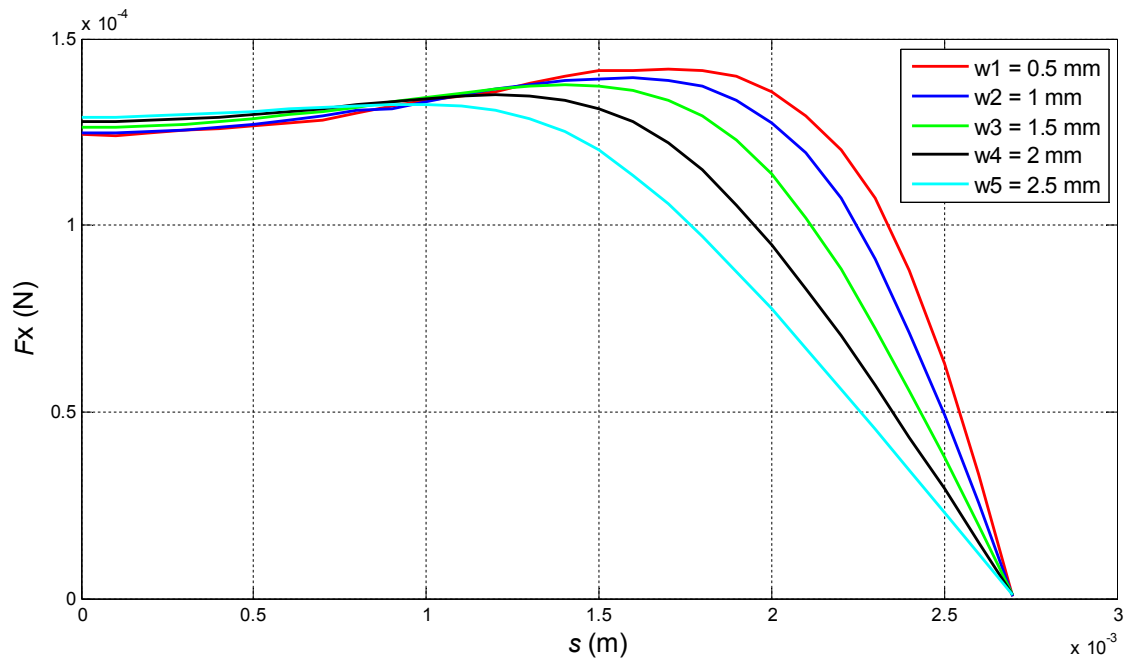


Fig. 15. Results obtained on the general model. Graph shows dependence of the magnetic  $x$ -axis force on the one-step shift with changing wire-gap ratio. Shift for each course is done by one step from the excited to the non-excited coil.

Fig. 15 clearly demonstrates the trend declaring that the maximal force effect is dependent on the wire width. More precisely, the smaller the width, the higher the force. The reason behind this is reducing conductor cross section, which increases the current density and as result also the resultant magnetic force. The same trend shows force courses in the  $z$ -direction in Fig. 16.

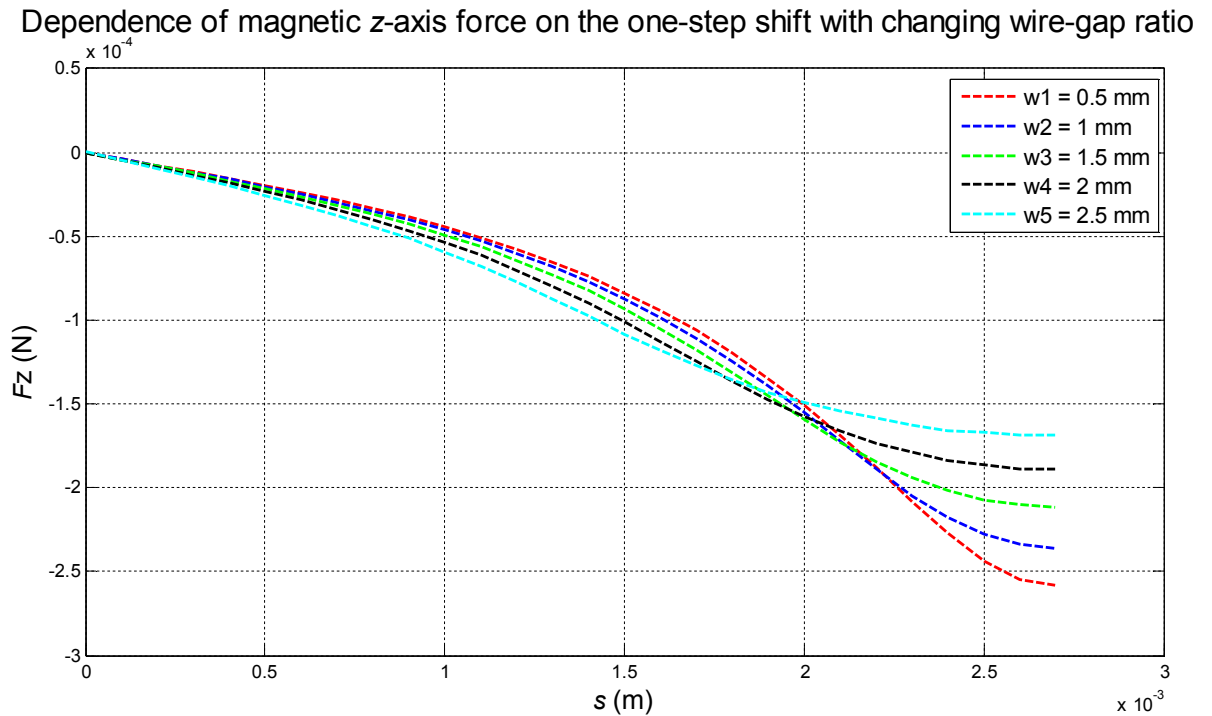


Fig. 16. Results performed on the general model. Graph shows dependence of the magnetic z-axis force on the one-step shift with changing wire-gap ratio. Shift for each course is done by one step from the excited to the non-excited coil.

Due to results shown above, for further design of *Scarabeus* platform the smallest wire width possible was chosen. The smallest wire width was determined by the minimal production capability standard stated on the manufacturer's website, which is 0.12 mm. The magnet width was given by the smallest magnets (1x1 mm), which are freely available on the market. Insulation gap dimension was then calculated by equation (7). The wire height was chosen according to the same rules as height, but with consideration of its current load capacity and thermal properties (35  $\mu\text{m}$ ). Geometric parameters for control simulations were summarized in Table. 3. For each parameters we performed control simulations shown in Figs. 17 and 18.

Tab. 3. *Scarabeus*'s geometric parameters used in simulations.

Scarabeus platform				
width [mm]			height	
$m$	$w$	$g$	$w$ [ $\mu\text{m}$ ]	$m$ [mm]
1	0,12	0,38	35	1
	0,18	0,32		
	0,24	0,26		
	0,3	0,2		
	0,38	0,12		

Dependence of magnetic x-axis force on the one-step shift with changing wire-gap ratio

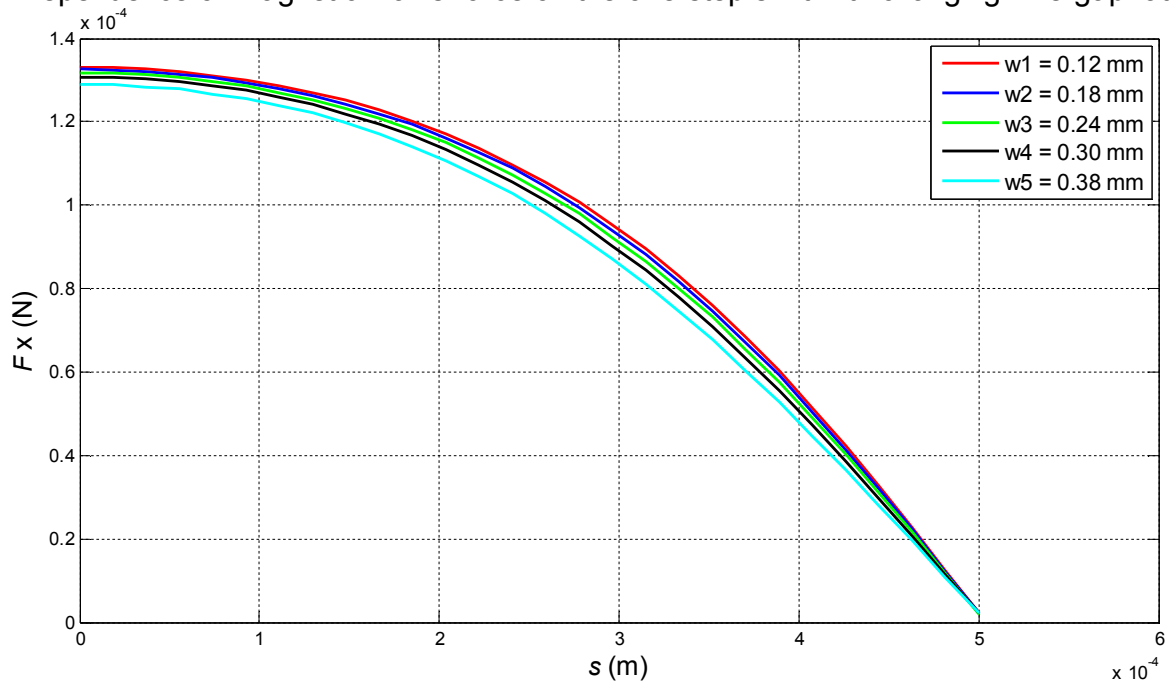


Fig. 17. Results performed for the proposed dimensions of *Scarabeus* platform. Graphs show dependence of the magnetic x-axis force on the one-step shift with changing wire-gap ratio.

Shift for each course is carried out by one step from the excited to the non-excited coil.

Dependence of magnetic z-axis force on the one-step shift with changing wire-gap ratio

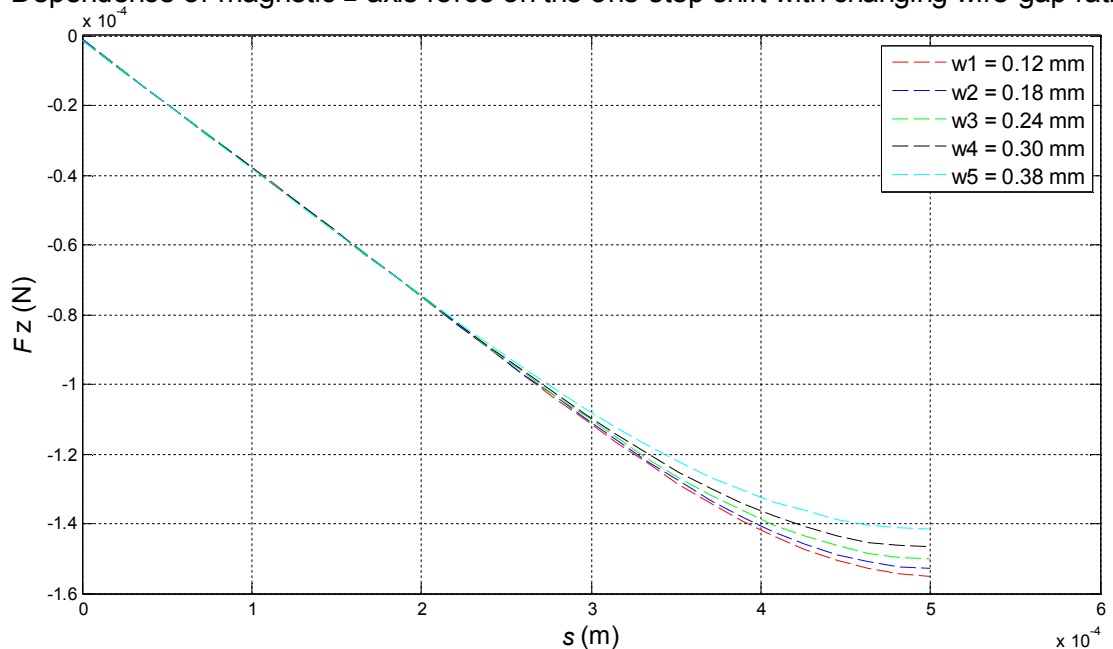


Fig. 18. Results performed for the proposed dimensions of *Scarabeus* platform. Graph shows dependence of the magnetic z-axis force on the one-step shift with changing wire-gap ratio.

Shift for each course is carried out by one step from the excited to the non-excited coil.

Control results established in the Fig. 17 and 18 performed for *Scarabeus* platform show different courses of magnetic force than the general model illustrated in the Figs. 15 and 16. After another performed simulations, which is not included in this work has proven that for course curving the magnet height is responsible. On the other side, obtained knowledge (shown in the previous chapter for the general model) was implied also for the *Scarabeus* system and, therefore, its successful process of force maximization could be started.

## 4.2 Mathematical model of motion

All developed platforms are using same mathematical model for motion of the robots [7], which comes from motion equation.

$$\mathbf{F} = m \cdot \frac{d^2 \mathbf{s}}{dt^2}, \quad (9)$$

where  $\mathbf{F}$  is the force,  $m$  is the mass,  $\mathbf{s}$  is the trajectory and  $t$  is the time. Equation can be simplified to

$$\mathbf{F} = m \cdot \frac{d\mathbf{v}}{dt} = m \cdot \mathbf{a}, \quad (10)$$

where  $v$  is the velocity and  $a$  is the acceleration.

Resultant force is made by vector sums of following forces

$$\mathbf{F} = \mathbf{F}_{Mx} + \mathbf{F}_{Mz} + \mathbf{F}_t, \quad (11)$$

where  $\mathbf{F}_{Mx}$  and  $\mathbf{F}_{Mz}$  are electromagnetic forces in  $x$  and  $z$  directions composed of Maxwell and Lorentz forces, and  $\mathbf{F}_t$  is friction force.

The system works mainly on the centrifugal Lorentz force effect, which is applied on the activated coils by PMs, but also with almost negligible Maxwell forces. Thus, if electromagnetic force is greater than the frictional force, robot starts controlled movement. The frictional force is defined as

$$F_t = k \cdot m \cdot g, \quad (12)$$

where  $k$  is the coefficient of shear friction and  $g$  is the gravitational constant.

### 4.3 Robot body design

As has been stated in the Chap 2.1.1, the platforms utilizes the interaction of the magnetic fields created by coils and PMs. The real reason behind this technique is represented by great properties of neodymium magnets, which grant great force effect due to their low weights.

The first generation of robot's prototypes were manufactured with same technology as robots for *MagStriver* platform from the plastic profiles created to fit one or four magnets. Profiles were printed by 3D printer Original Prusa i3 MK2S from PLA material. Designed dimensions of the robot with one PM were 1.5 x 1.5 x 1.2 mm and with four PMs the dimensions were 3.2 x 3.2 x 1 mm. Due to small profile proportions, 3D printer could not print very precise profiles and that led to four-bot's poor performance with very high error rate.

Next generation of robots (Fig. 19) were created by Ing. Jiří Kuthan using a CNC machine with very high precision and robot's error rate drastically decreased. The dimensions of plastic profiles are 3.5 x 3.5 x 1 mm with a weight around 0.0075 g and could contain 4 to 9 permanent magnets. Possibility to fit profiles with this many magnets enables opportunity to create robots with different abilities by combining multiple magnets and their polarity. (Polarity of magnets determines the movement direction.) As material for carrier profile a high-impact polystyrene *Anwindur* was used. As ferromagnetic bodies we used cylindrical shaped neodymium permanent magnets (VMM7-N42) with weight 0.006 g and  $(BH)_{\max}$  318–350 kJ/m<sup>2</sup>.

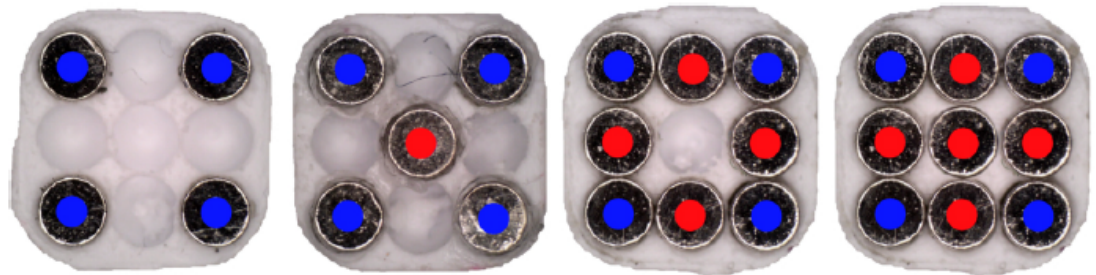


Fig. 19. Different types of robots: each robot shows different movement abilities due to arrangement of magnets. Magnet polarity orientation is distinguished by colour code. Blue means south from bottom view and red north. [8]

## 5 Scarabeus platform specification

The main objective behind the design of *Scarabeus* system, as it was stated in the beginning of Chap. 4, is dimension minimization, force maximization and functionality verification based on the parametric analysis. This chapter summarizes properties, platform dimensions, control electronics and algorithm, experimental verification, and is closed by comparison of the prototypes. Also it has to be noted that the systems represent continuation of its older prototype generation *MagStriver* and do not solve problems of independent parallel magnetic actuation of MAS.

The platform is illustrated in the Fig. 20. The working area is 75x80 mm and can control robots described in the Chap. 4.3.

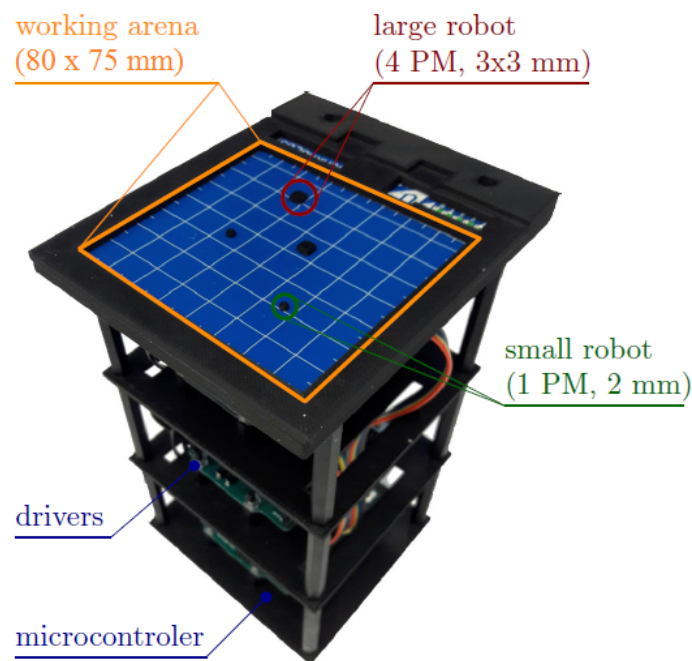


Fig. 20. Prototype of *Scarabues* module. [9]

Layout illustration is shown in Fig. 21 and the basic parameters are listed in Table 4. *Scarabeus* PCB contains four coils inputs and outputs. Two coils are for each direction and it is also possible to engage indication LEDs. The designed dimensions of parameters and properties are given in Table 4.

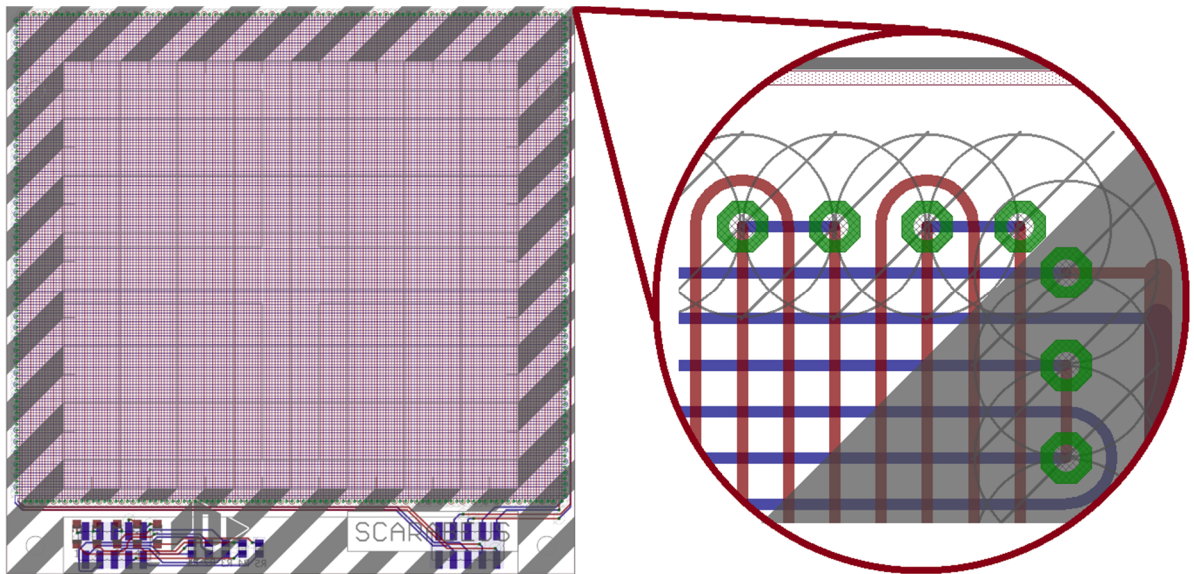


Fig. 21. Layout of *Scarabeus* module and its detail. Red coils enable movement in  $x$  direction and are situated in the top layer of PCB. The opposite blue coils enables movement in  $y$  direction and are situated in the bottom layer of PCB.

Tab. 4. Basic parameters of *Scarabeus* prototype.

Basic prototype parameters	Value			
Wire width	0.12 mm			
Insulation gap width	0.38 mm			
Layer gap height	0.1 mm			
Wire height	35 $\mu\text{m}$			
Working area width	80 mm			
Working area height	75 mm			
Coils parameters	$x_1$ -direction	$x_2$ -direction	$y_1$ -direction	$y_2$ -direction
Resistance	45.46 $\Omega$	45.11 $\Omega$	40.3 $\Omega$	40.11 $\Omega$
Length	8504 mm	8503 mm	8435 mm	8434 mm
Inductance	few $\mu\text{H}$	few $\mu\text{H}$	few $\mu\text{H}$	few $\mu\text{H}$

## 5.1 Principle of robot control

The basic field actuation principle is illustrated in Chap. 2.1.1., but it will also be described here in more detail. Figure 22 A) illustrates an example of field actuation switching sequence in the  $x$ -direction for which coils  $L_1$  and  $L_2$  are used. B) It represents cyclic switching sequence of coils. [8]

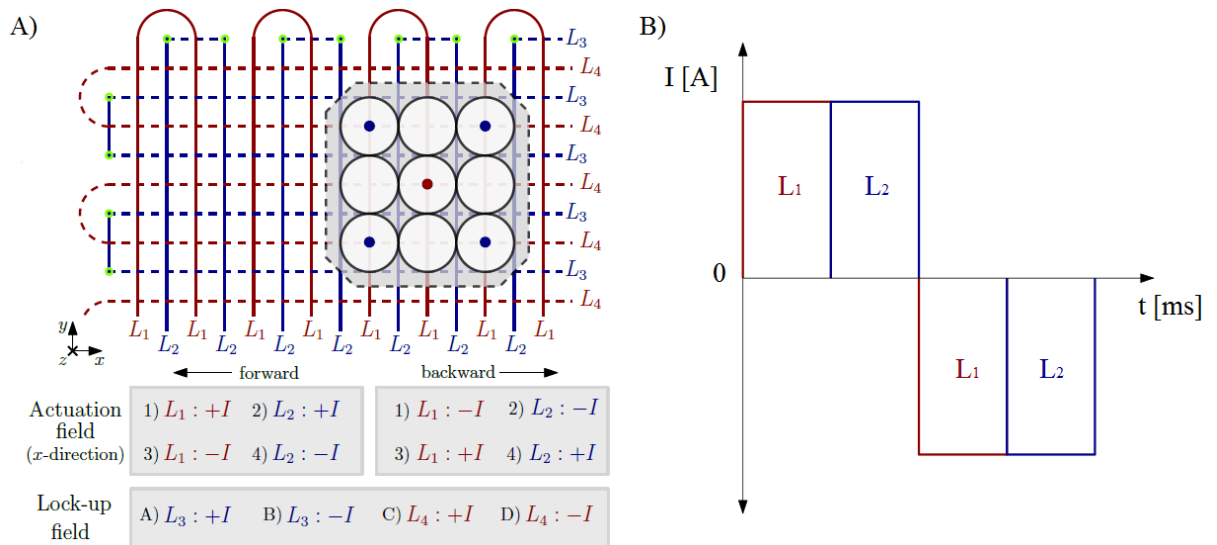


Fig. 22. A) Illustration of coplanar coils arrangement in two layers and also 5 permanent magnet-robot layout (dots in the middle of cylindrical magnets illustrate the magnet orientation). Top layer is indicated by full lines and serves for actuation in  $x$ -direction. Bottom layer indicates dashed lines which enables actuation in  $y$ -direction. A table with caption “Actuation field” explains switching sequence in  $x$ -direction. Second table called “Lock-up field” represents 4 possibilities of creating *lock-up field*, which have to be constant in time. Taken from [8]. B) Switching sequence of  $x$  forward direction with indication of excited coils and current orientation.

Movement of the robot is achieved by sequential excitation of two coils for each direction. Example shows (Fig. 22.) field actuation in  $x$ -direction, where for forward movement at first a positive current to the coil  $L_1$  needs to be applied which shifts robot to the non-powered  $L_2$  (motion direction is determined by a permanent magnets orientation). In this moment it is applied positive current  $+I$  into the input of  $L_2$ . Then robot is again pushed to the position of coil  $L_1$ , but now, because of the meandrical coil design  $L_1$ , input needs to be supplied by negative current  $-I$  in order to preserve robot in forward motion (in reality, current flow in the coil  $L_1$  is positive). Robot is then again pushed about one step to  $L_2$  where process with negative input current  $-I$  is repeated. This four-step switching sequence is then periodically repeated until the motion is stopped. Also, for a better explanation of current flows there serves Fig. 23 showing current flow direction in each fold. [8]

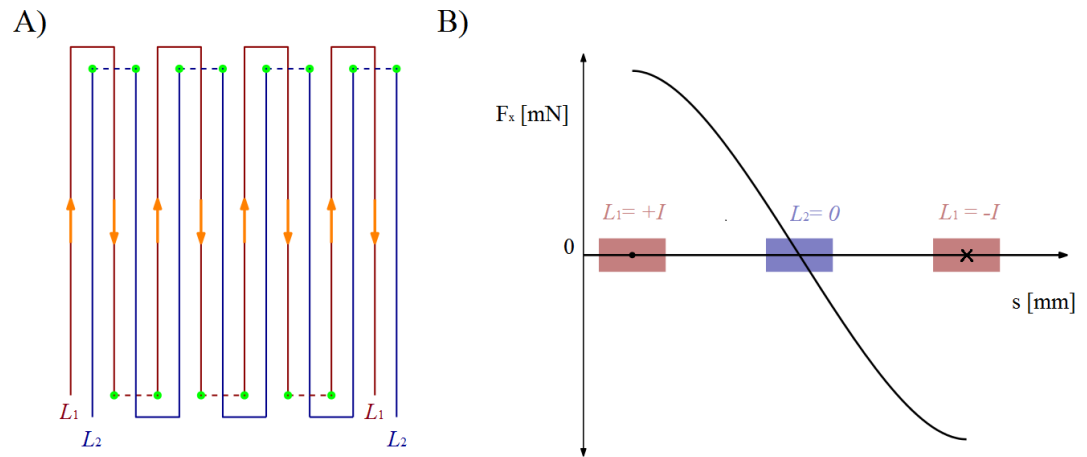


Fig. 23. A) Influence of meandering design on the current orientation on the coil  $L_1$ . The current direction is indicated by the orange arrows. B) Force effect in  $x$  direction created by excited coil  $L_1$  which pushes robot to the zero force point/line of coil  $L_2$ . If robot oversteps, force effect of opposite current orientation ( $L_1 = -I$ ) shifts robot back under the  $L_2$ .

In the illustrated example (Fig. 22 A) and Fig. 24) *lock-up field* is used by one of the coils  $L_3$  or  $L_4$  which currently do not serve to the robot movement in  $y$ -direction. By exciting one of the  $y$ -oriented coils, for example coil  $L_3$  for longer time period (current orientation is not important for *lock-up field*), the coil  $L_3$  will create forceful act of the stationary magnetic field, which firstly pushes the robot to the traces of non-powered coil  $L_4$  (zero force line) and secondly if robot starts to move freely in  $x$ -direction ( $L_1$  and  $L_2$ ) zero force rails in position of coil  $L_4$  created by force acts of  $L_3$  eliminate its unwanted movement in  $y$ -direction. Thus, if *field actuation* in both direction is required, *lock-up field* cannot be applied. *Lock-up field* is possible to use only when the robot is moving strictly in the  $x$  or  $y$  direction.

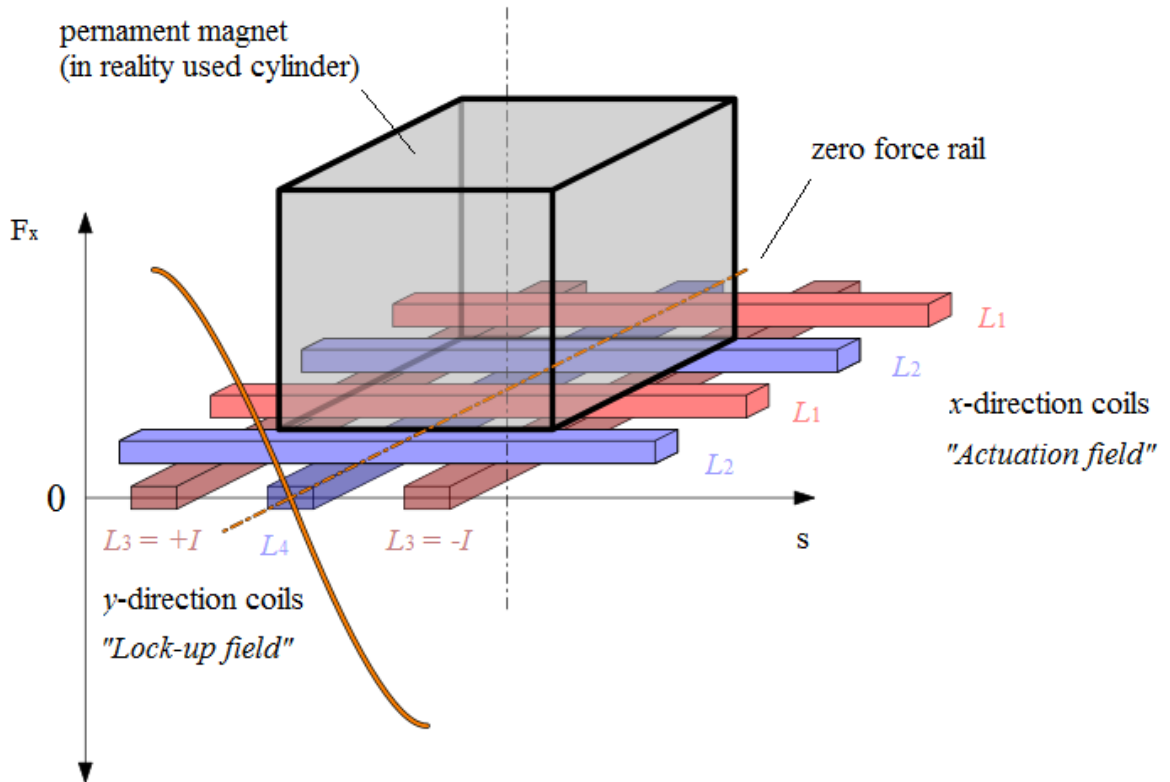


Fig. 24. Image illustrates explained example of *field actuation* in  $x$ -direction ( $L_1$  and  $L_2$ ) and *lock-up field* in  $y$ -direction ( $L_3$  and  $L_4$ ). The excited coil  $L_3$  creates by its magnetic force zero force rail in position of  $L_4$  where PM is moving without unwanted motion in  $y$ -direction.

## 5.2 Hardware and control algorithm

As a control unit *Arduino Uno* was employed with extension of two *Arduino Motor Shields* used as drivers. Motor shields contains two H-bridge units, which are able to power coils in positive and also negative currents. Each H-bridge enables control over one coil. For more user friendly actuation an analogue *Arduino Joystick PS2* periphery was added.

A flowchart of the control algorithm will not be included, because of the code simplicity. The code is attached on the CD. The algorithm firstly establishes functions for the forward and backward movements in  $x$  and  $y$  directions according to adequate coil switching cyclic sequence. Then, the position of *Arduino Joystick PS2* is continuously scanned and this information is used for executing appropriate movement functions.

### 5.3 Experimental verification

Experimental verification is done on the *Scarabeus* platform with usage of last generation of precise CNC made robots shown in Chap. 4.3. Motion tests are beyond the diploma thesis frame and were done by Ing. Martin Juřík and Ing. Jiří Kuthan. Tests are focused on the accuracy of robot motion, two robots interaction and influence of ferromagnetic barrier on the robot's body. [8]

#### 5.3.1 Robot motion analysis

First test shows accuracy results and smoothness of the robot movement, which is influenced by applied voltage  $U$  and time of one robot step  $t_s$  corresponding to its speed  $v$ . Results of robot accuracy movement along triangular trajectory for constant voltage  $U = 17$  V with different step times  $t_s$  are shown in Fig. 25. [8]

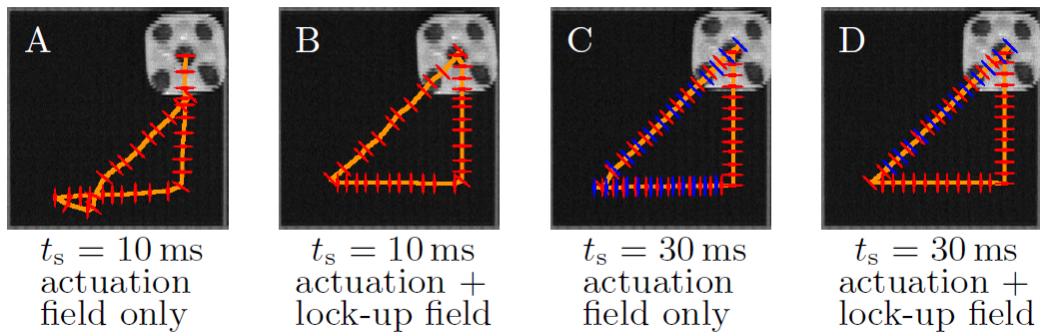


Fig. 25. Testing of robot movement on a triangular trajectory with constant voltage  $U = 17$  V and different step times  $t_s$ . Red lines show starting movement from the starting point and blue lines indicate overstepping of the zero-force point. Robot shivers only when blue lines are present. Otherwise robot stops where it should. Taken from [8].

Test is made for two step times 10 ms (A and B) and 30 ms (C and D) with basic field actuation (A and C) and with *lock-up field* (B and D). If step time is too low, the robot manifests high inaccuracy and error rate due to too high system dynamics. It is caused by robots incapability to synchronize with short time step, mainly while accelerating and changing of the motion direction, but also while stabilizing itself in equilibrium position of each step. [8]

Inaccuracy of low step time (A) could be partly limited by actuation with *lock-up field* (B). Unfortunately, actuation with *lock-up field* could be used for now only for movement strictly in  $x$  or  $y$  direction. The diagonal part of triangle uses actuation without *lock-up field*. [8]

Another way how to improve accuracy is the increase of the step time  $t_s$ . (C and D) However, it has to be stated a high voltage and low step time at the same time causes higher

rate of robot shivering. Shivering is illustrated by blue lines in Fig. 25 (C and D). The reason behind this phenomenon is a very fast acceleration of robot which leads to overstepping non-excited coil, where a zero-force point is placed. And beyond the zero force point the opposite force kicks robot back. This is repeated until robot is in the stabilized position or starts the next step. [8]

### 5.3.2 Interaction between two robots

Mutual influences of two robots are shown in Fig. 26. Experiment is done for two robots which attract one another (A+B) and two robots which repel each other (C+D). Also, tests were again different due to actuation field only for (A) and (C) and actuation with lock-up field for (B) and (D). [8]

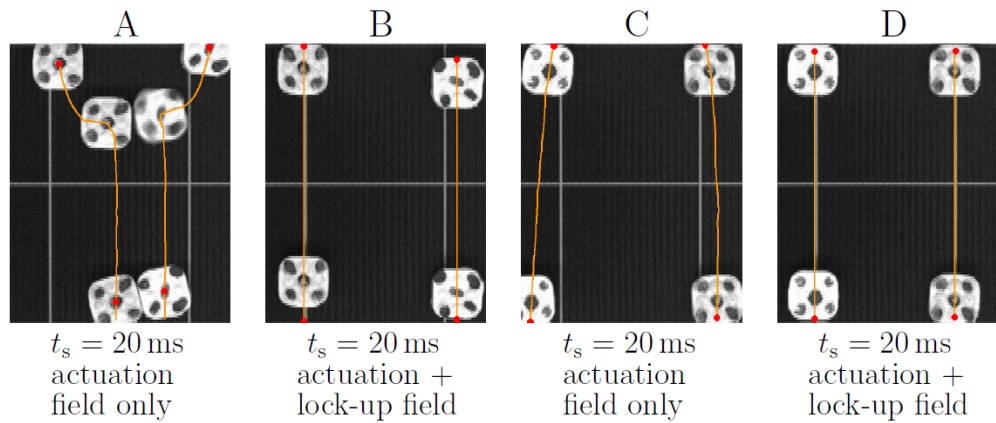


Fig. 26. Measurement of two robots mutual interaction with voltage  $U = 17$  V. (A) and (B) shows attracting orientation. (C) and (D) shows repelling orientation. Taken from [8].

Experiment results (Fig. 26) are very obvious especially with impact of the *lock-up field*. If *lock-up field* is activated, robots could be much more close to each other and almost without mutual influence (B) and (D). In the opposite actuation without *lock-up field* they strongly repel (C) or attract robot (A). Attracting variant could lead to problematic robots collision or even worse crash (Fig. 27). After crash robots are not able to move until they are manually split. [8]

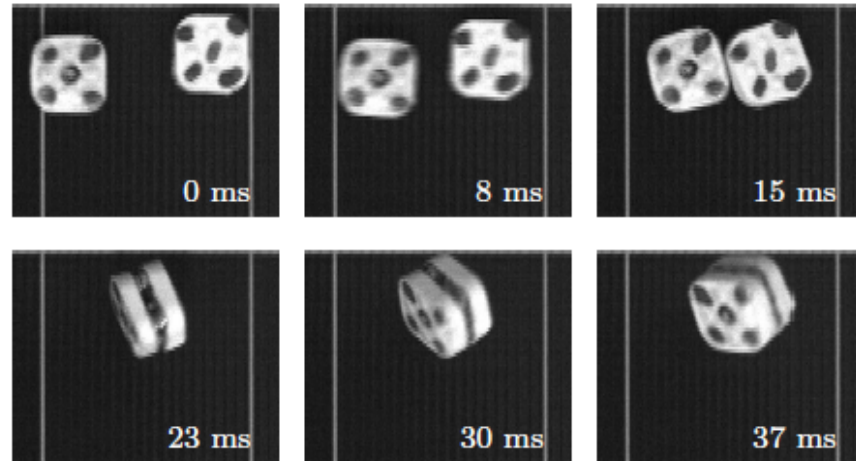


Fig. 27. Crash between two robots with time step  $t_s = 20$  ms and input voltage  $U = 17$  V.

Taken from [8].

### 5.3.3 Interaction between robot and ferromagnetic body

Similar test on the effects of actuation with *lock-up field* was done with robot and ferromagnetic barrier and the results are shown in Fig. 28. Motion with actuation field only shows high inaccuracy until robot is attached to ferromagnetic body (A and C). On the opposite robot *lock-up field* is active showing great actuating properties and influence of ferromagnetic barrier is almost eliminated. [8]

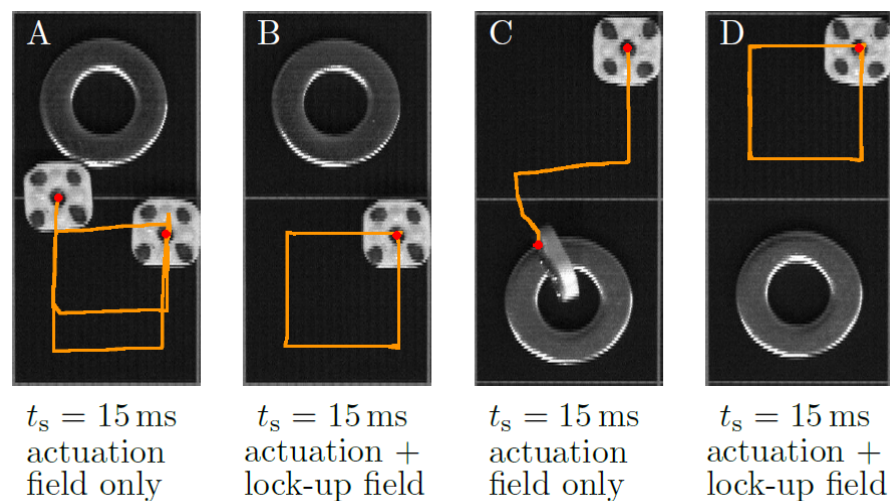


Fig. 28. Interaction between robot and ferromagnetic barrier with time step  $t_s = 15$  ms and input voltage  $U = 17$  V. Taken from [8].

### 5.3.4 Identification of dynamic characteristics

The results of dynamic measurement are summarized in Fig. 29 which shows dependency of minimal input voltage  $U$  and performance  $P$  on the robot velocity  $v$ . Robot speed is set up by step time  $t_s$ . The lower the step time, the higher the velocity. Also increase of the input voltage leads to the higher force effect and robot speed. If input voltage is too high and step time too low, the robot starts to shiver and cease to be effective. Shivering is assigned to the red zone. [8]

Results show that maximal velocity for specific voltage level is dependent on the robot design. Design is given by different combinations and numbers of PMs. Robots with higher numbers of PMs than 5 showed up to have lower maximal speed and even through better magnetic properties could not beat top speed of 5 PMs robot. This effect is given by the higher impact of magnets weight than improvement of robot magnetic properties. Maximal measured speed of robot with 5 PMs was 50 mm/s. [8]

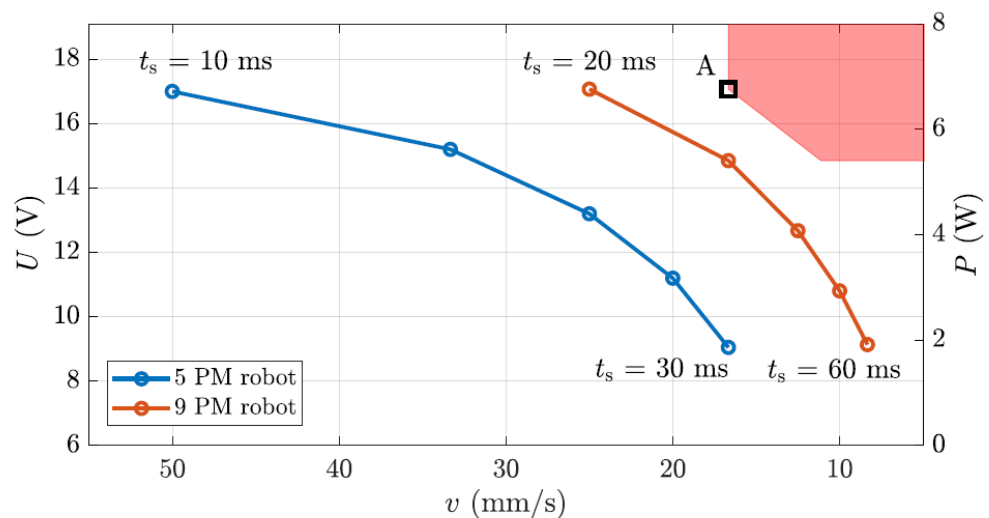


Fig. 29. Dependency of coil performance  $P$  and voltage  $U$  on the robot velocity  $v$ . Red area represents parameters where actuation force is too high and robot starts to shiver. Point A represents testing of robot motion presented in the Fig. 25 (C)+(D). Taken from [8].

### 5.3.5 Analysis of transport capabilities

Figure 30 shows dependency of maximal percentage and corresponding mass robot load on the one step time  $t_s$  (Chap. 5.3.1, Fig. 25) with constant input voltage  $U = 17$  V. The graph contains comparison of actuation field only and actuation with *lock-up field*. (Chap. 5.3.1). The robot mass load  $m$  was increased for each step time  $t_s$  until movement of the robot started to be inaccurate. As expected, with the lower robot speed (higher step time  $t_s$ ) the maximal load that the robot could transport increase, until the breakpoint is reached. Maximal transported load comes even higher than 500% in both compared cases which is equal to the value of almost 200 mg. [8]

The comparison of results shows that field actuation only has higher capacity load about  $\pm 20$  mg (or approximately 10 %) for each step time value  $t_s$  than actuation with lock-up field. The reason behind it seems to be inaccurate robot manufacturing. Robot deviation then leads to interference with lock up field, which creates motion resistance and lowering of its capacity load. [8]

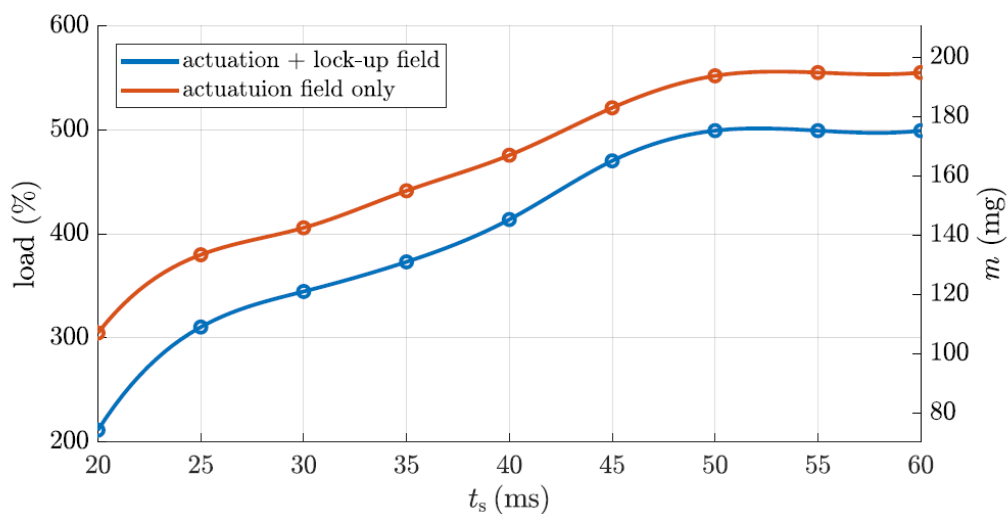


Fig. 30. Maximal percentile and corresponding robot mass  $m$  load in dependency on the step time  $t_s$ . Step time corresponds to robot speed, for example  $t_s = 20$  ms equals to 25 mm/s and 60 ms to 8.3 mm/s. Taken from [8].

#### 5.4 Comparison between *MagStriver* and *Scarabeus* platform

Results shown in Table 5 compare the robot and platform dimensions, coils parameters, robot weigh and its capacity load [13]. Also the results summarize that the stated objectives of dimension minimization and force maximization were successful. These statements declare dimension parameters and percent load capacity which achieve the mentioned objectives. However, force maximization greatly increases the coils resistance and with it undesirable Joule losses. Resistance is measured for differently long coil traces, more objective way of comparison would be through surface of cross-section, which is for *MagStriver* ( $S_M = 0.0175 \text{ mm}^2$ ) more than 4 times larger than that of *Scarabeus* ( $S_S = 0.0042 \text{ mm}^2$ ) and this means 4 times lower resistance. Because of high resistance of *Scarabeus* platform another parametric analysis was made in order to lower resistance of another platform *Isoptera* designed for multi-agenda. Design of *Isoptera* will be described in following chapters.

Tab. 5. Properties comparison between *MagStriver* and *Scarabeus* platforms [8] [13].

	<i>MagStriver</i>		<i>Scarabeus</i>	
<b>Parameters</b>	Values			
Wire width	0.5 mm		0.12 mm	
Gap width	0.25 mm		0.38 mm	
Thickness of insulation layer	0.1 mm		0.1 mm	
Robot weight	0.12 g		0.0315 g	
Maximal capacity load	0.41 g (400%)		<b>0.2 g (550%)</b>	
Robot dimension	8.6 x 8.6 mm		3.5 x 3.5 mm	
Wire height	35 um		35 um	
<b>Coil parameters</b>	x1	y1	x1	y1
Resistance	4,3 $\Omega$	4,1 $\Omega$	<b>45,4 <math>\Omega</math></b>	<b>40,3 <math>\Omega</math></b>

## 6 Design of *Isoptera* platform

Design of *Isoptera* builds on the results collated through *Scarabeus* platform (uses the same mathematical models and robots designs). The main goal of design was independent parallel electromagnetically guided actuation of multiple robots. As it was stated in research, possibilities of parallel movement are following:

1. different robot properties [14],
2. spatially selective magnetic field actuation (problematics of *force free point*) [15] and
3. separation of working area into self-controlled workspaces, so-called *segments*. [10][16]

First path and as the most attractive idea seemed to be spatially selective magnetic field actuation. The objective was creation of periodical so-called *force free point / line* inside the working area, where one robot can stand while others can be freely actuated. The objective tried to be achieved by adding another layer of coplanar coils which should create *force free points / lines* in some places of actuating grid. But after numerous attempts of simulations and coil design arrangement this idea was rejected. Reason behind rejection are following:

1. Unknown way to create a magnetic field with *force free point / line*.
2. Increase of energy consumption.

The work was then forced to choose second the most attractive technique. Which was separation of working area into the self-controlled *segments*, where could be independently controlled one robot, but also more robots simultaneously.

### 6.1 Coils resistance reduction

As it was stated in Chap. 5.4, high resistance leads to high energy consumption. In order to prevent generation the high Joule losses, another parametric analysis was performed, whose objective was to decrease resistance and also preserve or minimally lower the magnetic actuation force. The resistance is declared as

$$R = \rho \frac{l}{S}, \quad (13)$$

where  $R$  is the resistance,  $\rho$  is the resistivity,  $l$  is the length and  $S$  is the cross-section area of the conductor. For resistance decrease was we selected the cross-section  $S$ , which was the parameter that could most easily be influenced through the wire width and height. Force courses for different wire dimension are illustrated in Fig. 31.

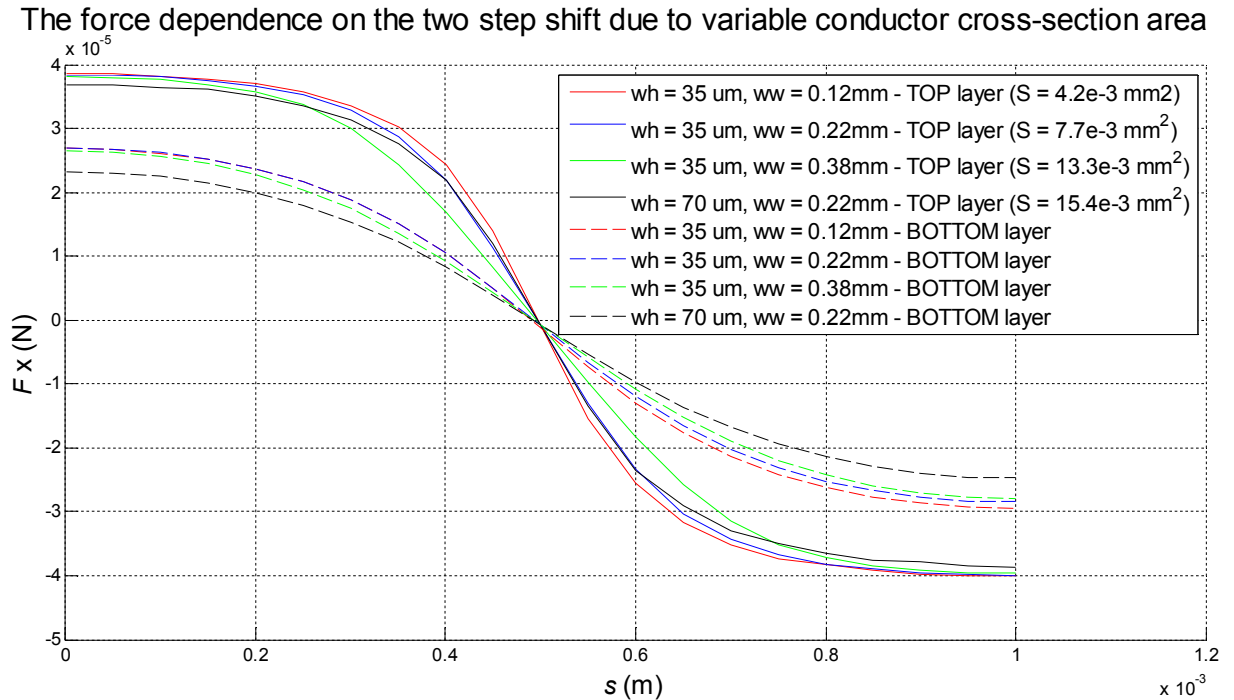


Fig. 31. Force dependence on the two step shift due to variable cross-section area of the conductor. Shortcuts  $wh$  means wire height and  $ww$  wire width. Red force courses match properties of the *Scarabeus* prototype. Full lines shows top layer and dashed bottom layer of PCB. Distance between layers is 0.1 mm.

As Fig. 31. Shows, red force courses match properties of the *Scarabeus* platform, with cross-section area  $S = 0.0042 \text{ mm}^2$ , which equals to wire height  $wh = 35 \text{ }\mu\text{m}$  and  $ww = 0.12 \text{ mm}$ . From simulation results, it can be seen that wire height has higher influence on force peak drop of the bottom layer than wire width with similar cross-section area. This is given by greater distance between PM and bottom layer about additional height of top layer. Because of this we prefer increasing of the cross-section area through the wire width.

Also it has to be noted that force drops for variable cross-section areas are minimal, while resistance decrease is enormous. This declares blue course ( $wh = 35 \text{ }\mu\text{m}$  and  $ww = 0.22 \text{ mm}$ ) having almost two times larger conductor cross-section area, but force peak remains almost unchanged due to *Scarabeus*'s force course ( $wh = 35 \text{ }\mu\text{m}$  and  $ww = 0.12 \text{ mm}$ ).

For *Isoptera*'s design we picked the following parameters:  $ww = 0.27 \text{ mm}$  and  $wh = 35 \text{ }\mu\text{m}$ , which equals to  $S = 0.00945 \text{ mm}^2$  and leads to resistance decrease more than two times due to original *Scarabeus*'s design ( $S = 0.0042 \text{ mm}^2$ ).

## 7 *Isoptera* platform specification

This chapter summarizes design properties, control block diagram, hardware, crossovers between *segments* and control algorithm. *Isoptera*'s experimental verification will not be included, because of the almost identical properties as *Scarabeus* platform (Chap. 5.3.1). Only attention to experimental verification will be focused on the crossings between *segments*.

Working area of *Isoptera* platform is shown in Fig. 32. The workspace dimensions are 75x80 mm. Parameters of upper two segments are 35x40 mm and lower 40x40 mm. The crossing between adjacent segments is 2 mm wide.

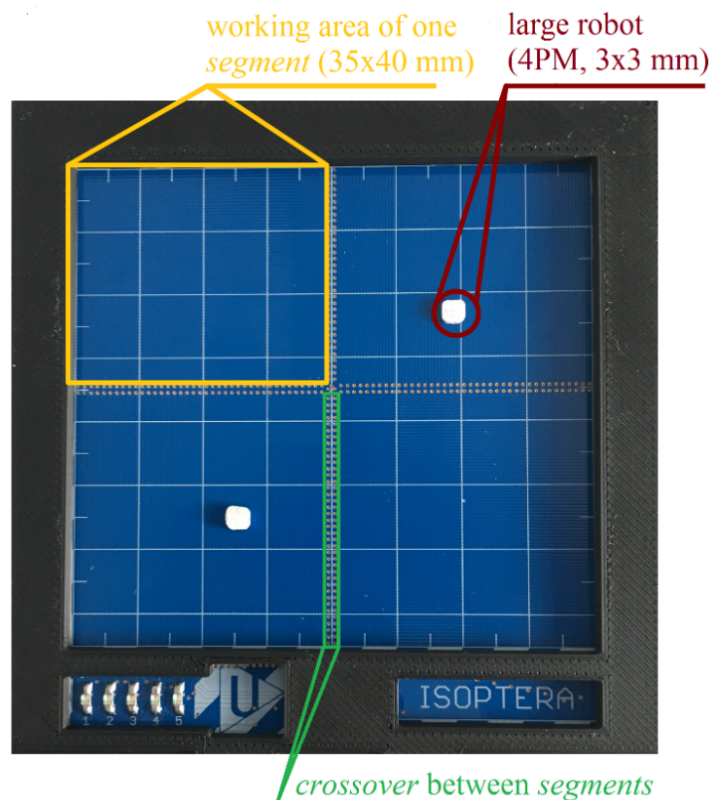


Fig. 32. Prototype of *Isoptera* platform.

The layout and crossovers detail design is illustrated in Fig. 33, corresponding properties and dimensions are then listed in Table 5. Also *Isoptera* platform has sixteen inputs and outputs. Each segment is then controlled through four inputs and outputs. For indication purposes we be used five LEDs in the left bottom corner.

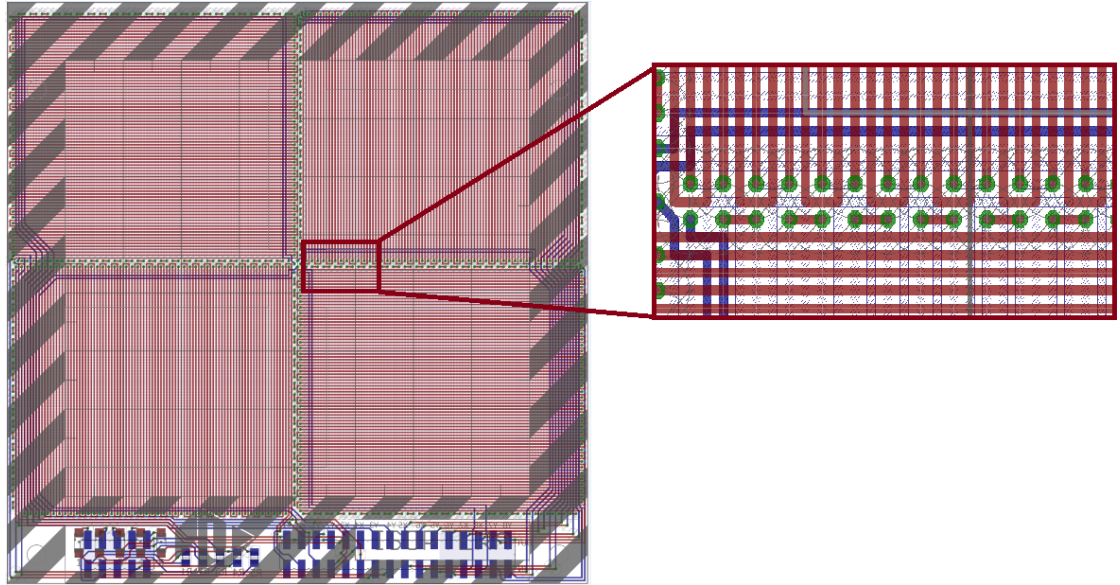


Fig. 33. Layout of *Isoptera* module and its detail. The PCB uses three layers layout. Red traces are situated in the top layer of PCB. The blue shredded lines are used for the middle layer and blue traces for the bottom layer of PCB.

Dimensions based on the parametric analysis are stated in Tab. 5. Coils resistance values are stated from the lowest to the highest measured value. Inductance was measured by two different measurement methods, the first one declaring value around  $1.6\mu\text{H}$  and another  $5.1\mu\text{H}$ .

Tab. 5. Dimensions and properties of *Isoptera* platform

<i>Isoptera</i>	
<b>General prototype parameters</b>	Value
Wire width	0.27 mm
Insulation gap width	0.23 mm
Layer gap height	0.1 mm
Wire height	35 $\mu\text{m}$
<b>Coils parameters</b>	Value
Resistance	4.1 - 4.3 $\Omega$
Inductance	few $\mu\text{H}$

## 7.1 Block diagram, hardware and control algorithm

Actuation of *Isoptera* prototype is based on optical localization of differently coloured robots. Currently, the system is designed for parallel independent actuation of two robots, each being controlled by one *Arduino Joystick JS2*. The system is illustrated in Fig. 34. The camera *PixyCam* localizes robots on the *Isoptera* working area and sends their signature and coordinates into a microcontroller. Illustration of *PixyCam* scanning is shown in Fig. 35. The *Arduino Mega* microcontroller then determines which segment of working area should be active for specific joystick. This information activates one of the eight targeted drivers *LN298P*, which through transistor logic (containing two H-bridges in each driver) power the coils in particular direction corresponding to signal from the particular joystick. Control algorithm flowchart for *Isoptera* platform is attached in the annex as Fig. 1.

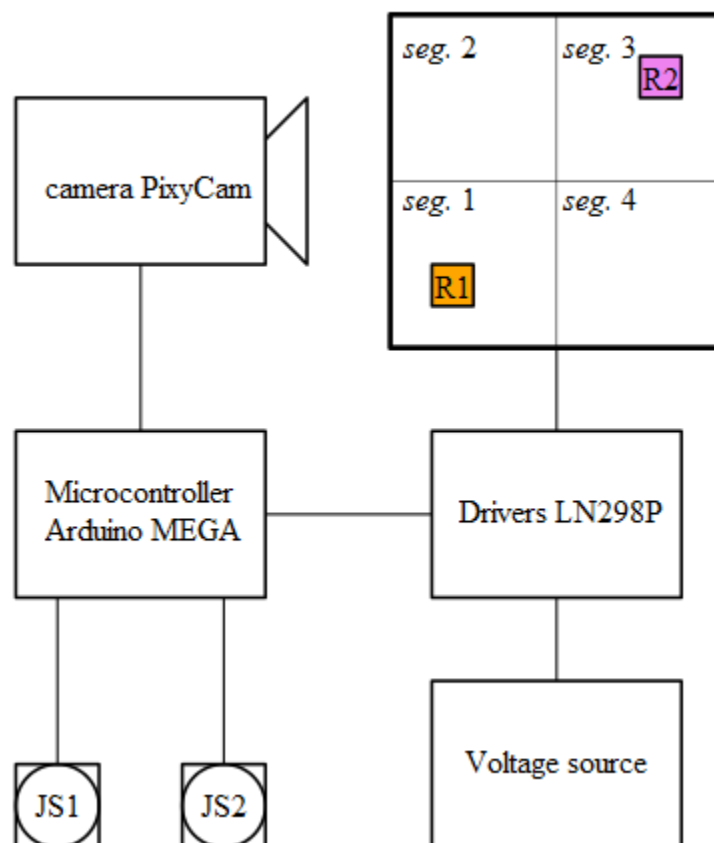


Fig. 34. *Isoptera*'s block control diagram.

The *PixaCam* camera scanning capability and resolution example is shown in Fig. 35. Robot signatures are distinguished by colour codes and each segment is defined in code through coordinates. Also it has to be noted, that camera's bad resolution and high light sensitivity causes problems with capturing the robots signatures.

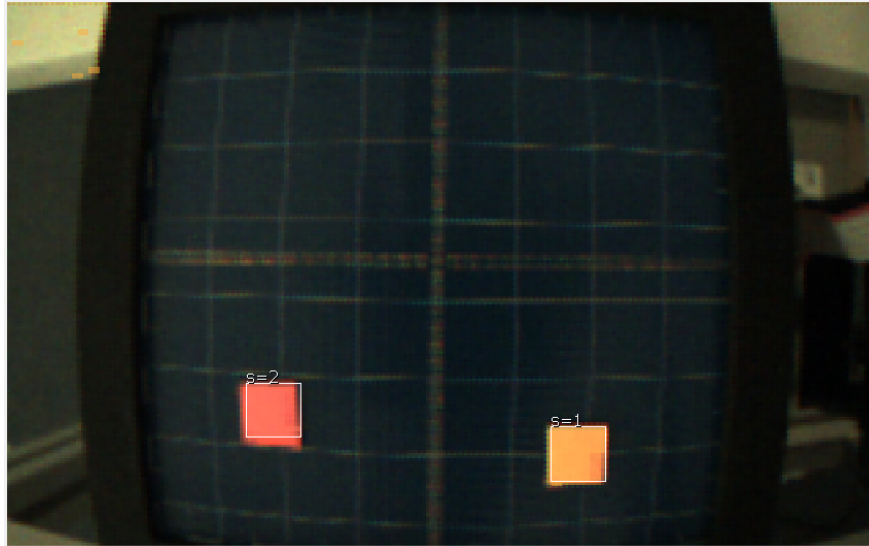


Fig. 35. A demonstration of the camera's scanning capability. Each robot is distinguished by its own colour code, which is assigned their individual signature.

## 7.2 Experimental verification of crossovers

This chapter summarizes transitions between different segments their design properties actuating methods and its principle. The biggest challenge of *Isoptera* platform were design of *crossovers* between different working areas so called *segments*. The gap between segments is 2 mm wide, which means three missing steps for basic actuation cycles. In the each crossover gap are fitted coils bends from two different segments. The middle head bends design created by two different coils makes so called *auxiliary coil*. Which could be also useful due to robot fluent transition. Detail is shown in the Fig. 36.

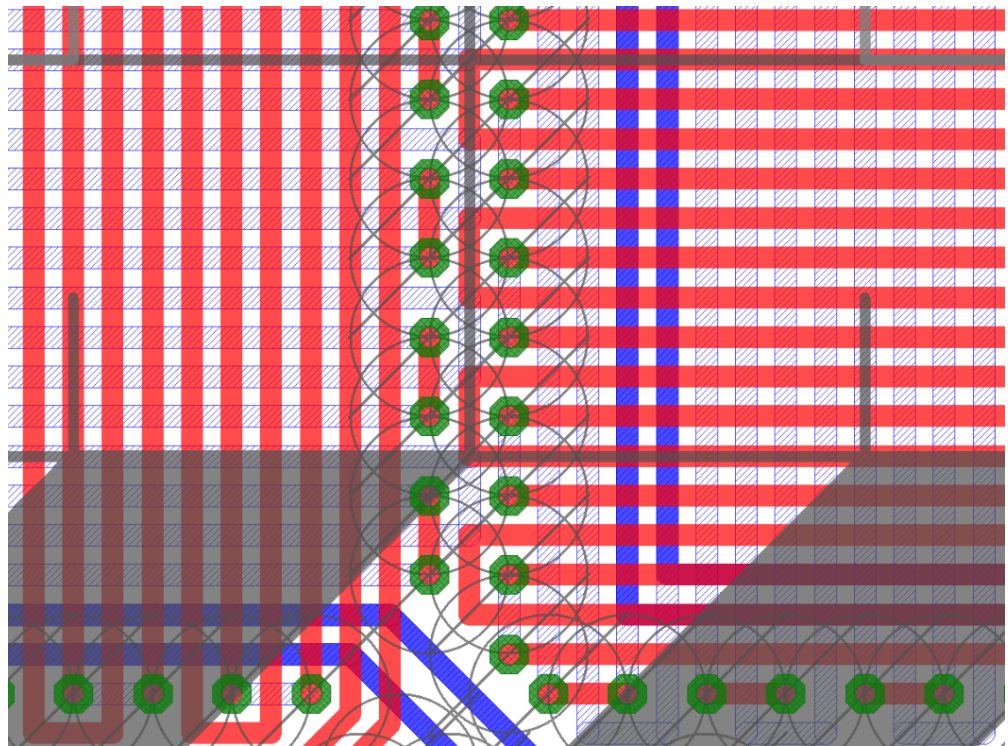


Fig. 36. Detail of *Isoptera*'s *crossover* between first (left) and fourth (right) segment. A gap width is 2 mm which means robot has to overcome three missing cycle steps. One step could be replaced by using middle head bends of two different coils.

The *Isoptera*'s design allows robots with at least 4 and 5 PM overcomes crossover with their own weight without problem even without use of *auxiliary coil* principle. There are only two conditions which must be observed and these are synchronized continuous actuation cycles of two segments where crossover is realized and movement prohibition other than perpendicular to the transition area. Successful transition declares videos of robots with 4 and 5 PM moving through all four segments attached on the CD and frames from the video are shown in Fig. 37. Principle and coil switching cycle are illustrated in Fig. 38.

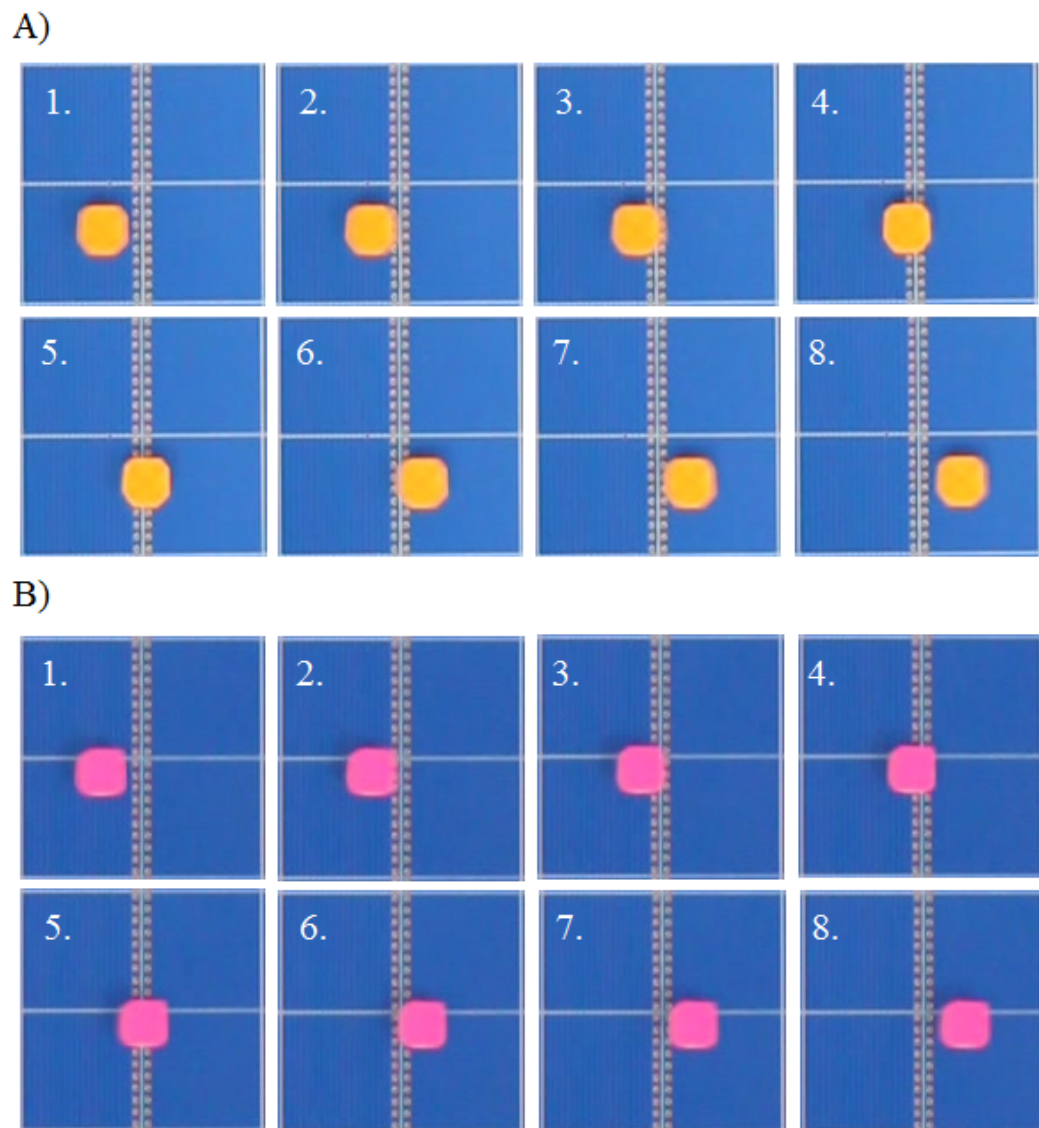


Fig. 37. Detail of successful passage between first (left) and fourth (right) segment. A) illustrates transition of orange robot with 5 PMs. B) passage of the pink robot with 4 PMs.

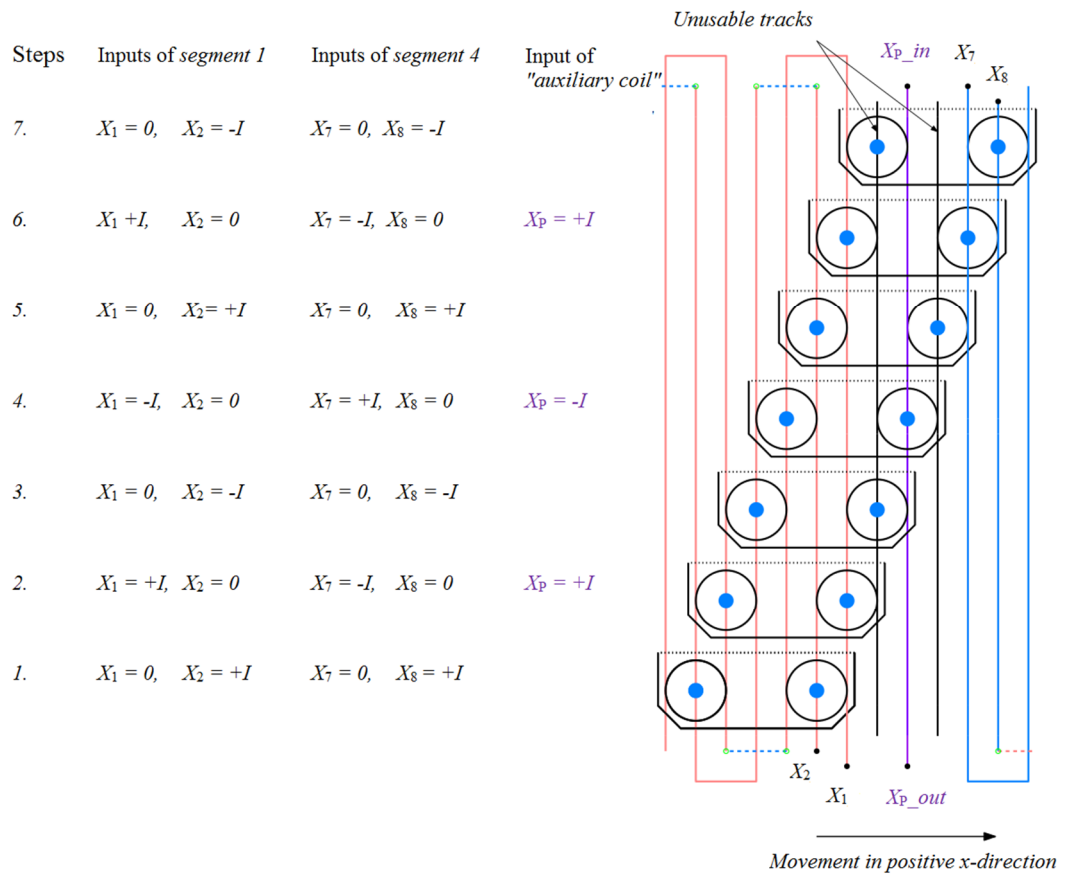


Fig. 38. Seven-step demonstration of how robot overcomes crossover between the first and fourth segments, while moving in positive  $x$ -direction. For each step the Table shows which coils have to be excited in order to fluently cross the gap. Robot with 4 and 5 PM with its own weight can surpass the gap without problem. A purple *auxiliary coil* is imaginary and in reality it is created by bends of coils  $Y_1$  and  $Y_7$  which alternately follow up. The *auxiliary coil* principle is further explained in Fig. 39. Black coils are *unusable tracks* where non-continuous  $y$ -oriented coils bends are focused.

Figure 38 illustrates how the robot overcomes the crossing area. Robot manages to overcome the crossing area, because one of its half is still above the working area one of the segments (step no. 3) This is enough for the robot to be pushed out to and gradually reach the unused half of the adjacent segment (step no. 6). Crossing is then repeated for the other half of the robot.

Since only half of the robot is working, it can be assumed that due to transition its load capacity will drop as well. The capacity load can be little bit increased by using a so-called *auxiliary coil* whose excitation can contribute to a smooth switching cycle and thus to slightly increase its normal working capacity again. It has to be noted that excitation of the *auxiliary*

coil, whose principle is illustrated in Fig. 39, can also decrease overall total capacity load because it is using principle of actuation with *discontinuous lock-up field*. Chap. 5.3.5 declares that actuation with *lock-up field* technique decreases maximal load capacity by about 10%. Also switching cycle of the *auxiliary coil* was stated in Fig. 38.

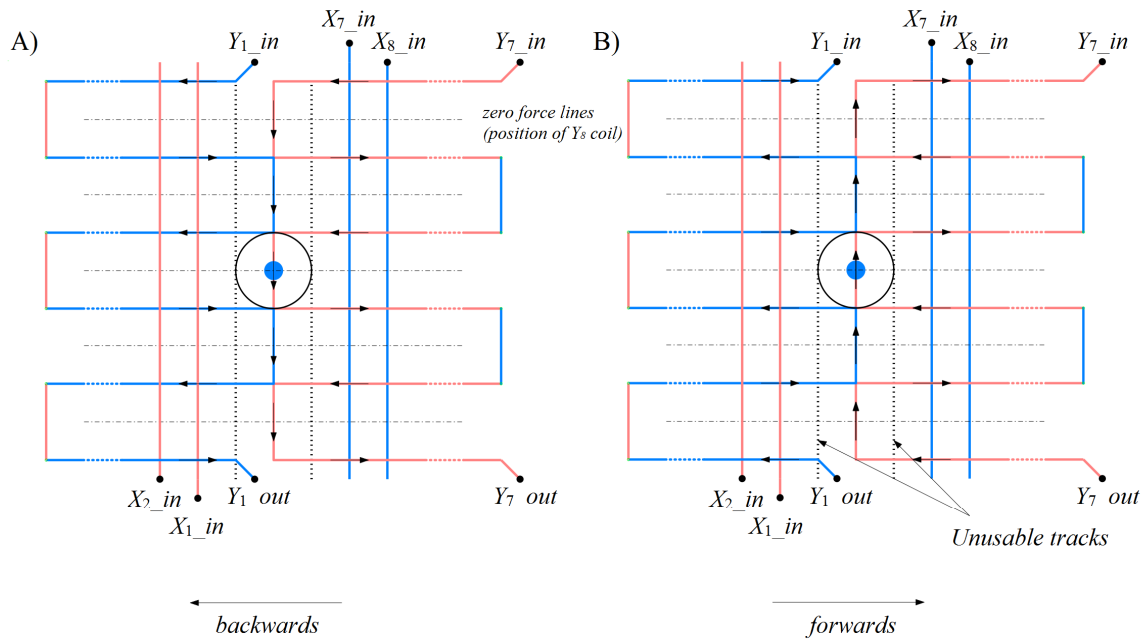


Fig. 39. Demonstration of the *auxiliary coil* principle, which combines smart design and *lock-up field* technique. A) Shows *auxiliary coil* positively excited ( $Y_1_{in} = +I$ ,  $Y_7_{in} = +I$ ), which will push the magnet backwards, while variant B) forward ( $Y_1_{in} = -I$ ,  $Y_7_{in} = -I$ ). Also while using *auxiliary coil* principle it is also used *discontinuous lock-up field*. Zero force (dash-dotted) lines are traces where coils  $Y_2$  and  $Y_8$  are placed. These coils cannot be used for *auxiliary coil* principle, because the design does not support it.

## 8 Conclusion

The main topic of the diploma thesis was aimed at problems of the independent parallel magnetic actuation of ferromagnetic bodies. On the development of the multi-agent systems, a great attention is currently focused.

First and second part of the thesis define basic concepts, main thesis motivations and state of arts where current platforms for magnetically guided actuation are described. Third part defines main thesis objectives, which is development of two platforms prototypes.

Part four describes the design of the *Scarabeus* platform through parametric analysis in software *Agros2D* [11] which deals with robot size minimization and platform step refinement to maximize the coils force effect on the robot. For this purpose, three studies were performed in total. The first one investigated the magnetic forces of the platform, namely Maxwell and Lorentz forces. The study revealed that for platform function only Lorentz force. Contributes significantly. Maxwell force is so low that its value can be neglected for further studies. (Chap. 4.1.1, Fig. 11) However, further studies consider the total magnetic force.

The second study dealt with the influence of magnet widths on the constant wire-gap ratio. Results have shown that platform can work for different magnet widths except the width covering the same number of positive and negatively excited coils. Next, it has been discovered a fundamental equation (4) (Chap. 4.1.2) for which the force effect is the highest. Also has to be noted that maximal force courses are repetitive in dependency on the specific magnet widths. On the mentioned equation it is based a study dealing with the influence of the variable wire-gap ratio. It was found that the smaller the wire cross-section area is, the greater the magnetic force of the platform is. On this knowledge, with respect to the current load, the *Scarabeus* platform was designed and manufactured.

The fifth part describes further principle of magnetic actuation with and without *lock-up field*, platform's properties, used electronic components, control algorithm and contains results of experimental verification (Chap. 5.3) done by Ing. Martin Juřík and Ing. Jiří Kuthan. Development of *Scarabeus* platform was closed by result comparison (Chap. 5.4, Tab. 5) with the older generation of *MagStriver*. The results of comparison declare successful fulfilment of the stage of two objectives. (Chap. 3)

The only disadvantage of the *Scarabeus* platform was the relatively high resistance. (Chapt 5.4, Table 5) A study dealing with reduction of the coil's resistance was performed, stated in the sixth part of the thesis describing the design of independent parallel positioning platform called *Isoptera*. The sixth part, as mentioned, summarizes the possibilities of independent parallel positioning and the reasons for the chosen way of solving the division of the working area into the so-called *segments*. It should be noted that each *segment* allows the independent movement of one robot.

The seventh part describes properties, block diagram, hardware, control algorithm, and successful solution of platform *crossovers*. Functionality and the ability to use *segmental* technique for parallel positioning declares video enclosed on the CD (Fig. 37) that demonstrates the smooth passage of a robot with five and four permanent magnets between adjacent independent *segments*.

The parallel positioning method of the *segment* system has been proved to be functional and could be further developed, especially due to the possibility of shapes modifying and adding of other working *segments* easily. On the other hand, the method disadvantages are a limit of the load capacity of the robot when it crosses between the adjacent *segments* and adding additional hardware elements, which also brings lesser system reliability.

## Further development

For the work continuation could be further developed better camera system with higher resolution for localization of the robots. Next step should be also further experimental verification of passage between segments with usage of *discontinuous lock-up field* stated in the Chap. 7.2, Figs. 38 and 39. Another area worth of development could be parallel kinematics of mechanically connected robots actuated independently inside their own *segments*. Or even better further research of techniques for independent parallel magnetic actuation without *segmental* distribution.

## List of literature and information sources

- [1] Microfactory. In: *Wikipedia: the free encyclopedia* [online]. San Francisco (CA): Wikimedia Foundation, 2001- [cit. 2018-05-22]. Available from: <https://en.wikipedia.org/wiki/Microfactory>
- [2] Multi-agent system. In: *Wikipedia: the free encyclopedia* [online]. San Francisco (CA): Wikimedia Foundation, 2001- [cit. 2018-05-22]. Available from: [https://en.wikipedia.org/wiki/Multi-agent\\_system](https://en.wikipedia.org/wiki/Multi-agent_system)
- [3] PELRINE, Ron, Annjoe WONG-FOY, Brian MCCOY, Dennis HOLEMAN, Rich MAHONEY, Greg MYERS, Jim HERSON a Tom LOW. Diamagnetically levitated robots: An approach to massively parallel robotic systems with unusual motion properties. In: *2012 IEEE International Conference on Robotics and Automation* [online]. IEEE, 2012, 2012, s. 739-744 [cit. 2018-05-23]. DOI: 10.1109/ICRA.2012.6225089. ISBN 978-1-4673-1405-3. Available from: <http://ieeexplore.ieee.org/document/6225089/>
- [4] MACH, František. *Magneticky ovládané robotické systémy pro mikromanipulaci* [online]. [cit. 2018-05-22]. Available from: [https://www.technickytydenik.cz/rubriky/veda-vyzkum-inovace/magneticky-ovladane-roboticke-systemy-pro-mikromanipulaci\\_42501.html](https://www.technickytydenik.cz/rubriky/veda-vyzkum-inovace/magneticky-ovladane-roboticke-systemy-pro-mikromanipulaci_42501.html)
- [5] HUSÁK, Miroslav. *Mikrosenzory a mikroaktuátory*. Prague: Academia, 2008. Gerstner. ISBN 978-80-200-1478-8.
- [6] FILIP, Jan. *Extension of the Control System for the Magnetic Manipulator with a Non-Flat Surface*. Prague, 2015. Diploma thesis. CTU
- [7] KUTHAN, Jiří. *Elektromagnetický systém pro polohování magnetických těles*. Pilsen, 2017. Diploma thesis. UWB
- [8] JUŘÍK, Martin, Jiří KUTHAN, Jiří VLČEK a František MACH. *Key Aspects of Magnetically Guided Actuation for Mesoscale Automation*.
- [9] IVAN, Ioan Alexandru, Gilgueng HWANG, Joel AGNUS, Micky RAKOTONDRABE, Nicolas CHAILLET a Stephane REGNIER. First experiments on MagPieR: A planar wireless magnetic and piezoelectric microrobot. In: *2011 IEEE International Conference on Robotics and Automation* [online]. IEEE, 2011, 2011, s. 102-108 [cit. 2018-05-23]. DOI: 10.1109/ICRA.2011.5979885. ISBN 978-1-61284-386-5. Available from: <http://ieeexplore.ieee.org/document/5979885/>
- [10] PELRINE, Ron, Allen HSU, Cregg COWAN a Annjoe WONG-FOY. Multi-agent systems using diamagnetic micro manipulation — From floating swarms to mobile sensors. In: *2017 International Conference on Manipulation, Automation and Robotics at Small Scales (MARSS)* [online]. IEEE, 2017, 2017, s. 1-6 [cit. 2018-05-23]. DOI:

- 10.1109/MARSS.2017.8001930. ISBN 978-1-5386-0346-8. Available from: <http://ieeexplore.ieee.org/document/8001930/>
- [11] KARBAN, Pavel., MACH, František., K, P., PÁNEK, David., DOLEŽEL, Ivo.: *Numerical solution of coupled problems using code Agros2D*, Computing, 2013, Volume 95, Issue 1 Supplement, pp 381-408, DOI [10.1007/s00607-013-0294-4](https://doi.org/10.1007/s00607-013-0294-4)
- [12] MACH, František. *Pokročilé metody a algoritmy pro analýzu sdružených úloh v elektromagnetismu*. Pilsen, 2015. Dissertation. UWB.
- [13] KUTHAN, Jiří a František MACH. *Magnetically Guided Actuation of Ferromagnetic Bodies on the Planar Surfaces: Numerical Modeling and Experimental Verification*. Pilsen, 2017.
- [14] DILLER, Eric, Joshua GILTINAN a Metin SITTI. Independent control of multiple magnetic microrobots in three dimensions. *The International Journal of Robotics Research* [online]. 2013, **32**(5), 614-631 [cit. 2018-05-23]. DOI: [10.1177/0278364913483183](https://doi.org/10.1177/0278364913483183). ISSN 0278-3649. Available from: <http://journals.sagepub.com/doi/10.1177/0278364913483183>
- [15] TONYUSHKIN, Alexey. Single-Sided Field-Free Line Generator Magnet for Multi-Dimensional Magnetic Particle Imaging. *IEEE Transactions on Magnetics* [online]. 2017, **53**(9), 1-6 [cit. 2018-05-23]. DOI: [10.1109/TMAG.2017.2718485](https://doi.org/10.1109/TMAG.2017.2718485). ISSN 0018-9464. Available from: <http://ieeexplore.ieee.org/document/7954650/>
- [16] CHOWDHURY, Sagar, Wuming JING a David J. CAPPELLERI. Independent actuation of multiple microrobots using localized magnetic fields. In: *2016 International Conference on Manipulation, Automation and Robotics at Small Scales (MARSS)* [online]. IEEE, 2016, 2016, s. 1-6 [cit. 2018-05-23]. DOI: [10.1109/MARSS.2016.7561741](https://doi.org/10.1109/MARSS.2016.7561741). ISBN 978-1-5090-1510-8. Available: <http://ieeexplore.ieee.org/document/7561741/>

# Annex

## Control algorithm flowchart of the *Isoptera* platform

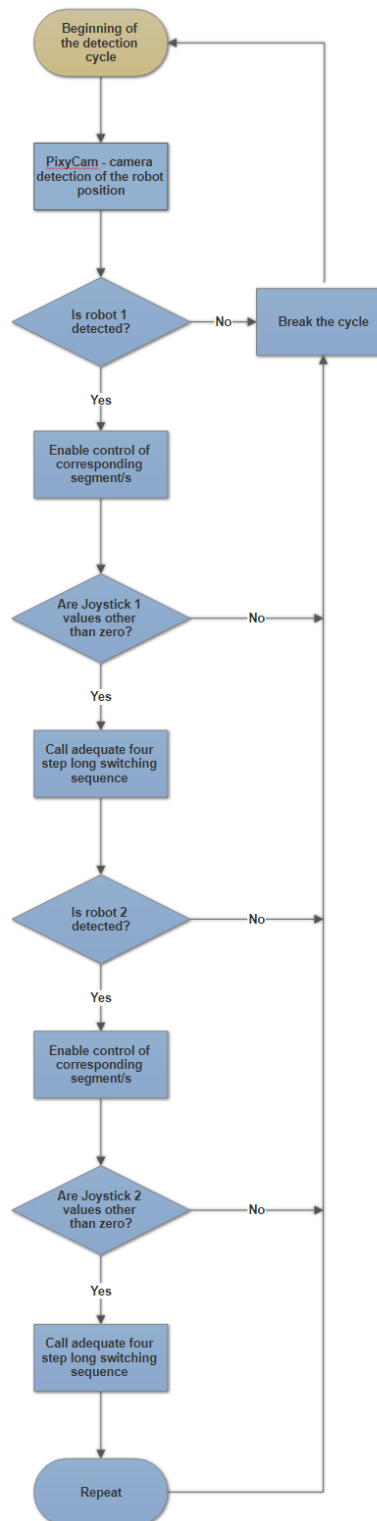


Fig. 1. Illustrates control algorithm flowchart of the *Isoptera* platform.